MNRAS **000**, 1–18 (2015) Preprint July 25, 2015 Compiled using MNRAS LATEX style file v3.0

Constraining AGN triggering mechanisms through the clustering analysis of active black holes

M. Gatti,[1] F. Shankar,[2] V. Bouillot,[3] N. Menci,[1] A. Lamastra,[1] M. Hirschmann,[4] F. Fiore[1]
[1]*INAF - Osservatorio Astronomico di Roma, via di Frascati 33, 00040 Monte Porzio Catone, Italy*
[2]*School of Physics and Astronomy, University of Southampton, Southampton SO17 1BJ, UK*
[3]*Centre for Astrophysics, Cosmology & Gravitation, Department of Mathematics & Applied Mathematics, University of Cape Town, Cape Town 7701, South Africa*
[4]*UPMC-CNRS, UMR7095, Institut d' Astrophysique de Paris, F-75014 Paris, France*

Accepted XXX. Received YYY; in original form ZZZ

ABSTRACT
The triggering mechanisms for Active Galactic Nuclei (AGN) are still debated. Some of the most popular ones include galaxy interactions (IT) and disk instabilities (DI). Using an advanced semi analytic model (SAM) of galaxy formation, coupled to accurate halo occupation distribution modeling, we investigate the imprint left by each separate triggering process on the clustering strength of AGN at small and large scales, at different redshifts and luminosities. Our main results are as follows: i) DIs, irrespective of their exact implementation in the SAM, tend to fall short in triggering AGN activity in galaxies at the center of halos with $M_h > 10^{13.5} h^{-1}\mathrm{M}_\odot$ (at all redshifts). On the contrary, the IT scenario predicts abundance of active, central galaxies that generally agrees well with observations at every halo mass. ii) The relative number of satellite AGN in DIs at intermediate-to-low luminosities is always significantly higher than in IT models, especially in groups and clusters. The low AGN satellite fraction predicted for the IT scenario might suggest that different feeding modes could simultaneously contribute to the triggering of satellite AGN. iii) Both scenarios are quite degenerate in matching large-scale clustering measurements, suggesting that the sole average bias might not be an effective observational constraint. iv) Our analysis suggests the presence of both a mild luminosity and a more consistent redshift dependence in the AGN clustering, with AGN inhabiting progressively less massive dark matter halos as the redshift increases. In light of our advanced models, we also discuss possible improvements on current AGN semi-empirical halo occupation modeling, as well as the impact of different observational selection cuts in measuring AGN clustering, including possible discrepancies between optical and X-ray surveys and redshift/luminosity effects.

Key words: galaxies: active – galaxies: evolution – galaxies: fundamental parameters – galaxies: interactions – cosmology: large-scale structure of Universe

1 INTRODUCTION

AGN are believed to be powered by the accretion of matter onto supermassive black holes (SMBHs)(Soltan 1982; Richstone et al. 1998). We also know that the masses of SMBHs in the local Universe relate to several properties of their host galaxies (Magorrian et al. 1998; Marconi & Hunt 2003; McConnell & Ma 2013; Kormendy & Ho 2013; Läsker et al. 2014). However, the physical mechanisms responsible for such intense accretion episodes in the galactic nuclei and their relation with the cosmological evolution of galaxies still remain unclear.

Various pictures have been proposed. One possible scenario envisages galaxy interactions as the main fueling mechanism. Gravitational torques induced by interacting galaxies would be effective in causing large gas inflows in the central region of the galaxy, eventually feeding the central SMBH. Luminous quasars are indeed often found to be associated with systems undergoing a major merger or showing clear signs of morphological distortion (Di Matteo et al. 2005; Cox et al. 2008; Bessiere et al. 2012; Urrutia et al. 2012; Treister et al. 2012). Less violent minor mergers or fly-by events have been invoked to account for moderately luminous AGN (Combes et al. 2009; Koss et al. 2010; Satyapal et al. 2014).

On the other hand, there is mounting observational evidence based on the star-forming properties and on the morphology of AGN hosts, suggesting that moderate levels of AGN activity might not be casually connected to galaxy interactions (Lutz et al. 2010; Rosario et al. 2012; Mullaney et al. 2012; Santini et al. 2012; Rosario et al. 2013; Villforth et al. 2014). Theoretically, *in-situ* processes, such as disk instabilities or stochastic accretion of gas clouds, have also been invoked as effective triggers of AGN activity (Dekel et al. 2009; Bournaud et al. 2011).

AGN clustering analysis could help to unravel the knots of this complex situation. Indeed, clustering measurements can provide vital information on the physics of AGN. Through the use of the 2-point correlation function (2PCF, Arp 1970) the spatial distribution of AGN can be effectively used to investigate the relation between AGN and their host halos, enabling to pin down the typical environment where AGN live. This in turn could potentially provide new insights into the physical mechanisms responsible for triggering and powering their emission.

For instance, clustering analysis of optically-selected bright quasars carried out at different redshifts (Porciani et al. 2004; Myers et al. 2006; Coil et al. 2007; Shen et al. 2007; Padmanabhan et al. 2009; White et al. 2012) have pointed out a typical host halo mass of the order of $logM_h[h^{-1}\mathrm{M}_\odot] \sim 12.0 - 12.5$, corresponding to the typical mass scale of galaxy groups. These observational evidences would add support to the interactions scenario, since in these environments the probability of a close encounter is higher (Hopkins et al. 2008; McIntosh et al. 2009).

Otherwise, a number of clustering studies on moderately luminous X-ray selected AGN (Coil et al. 2009; Hickox et al. 2009; Cappelluti et al. 2010; Allevato et al. 2011; Krumpe et al. 2012; Koutoulidis et al. 2013) have obtained higher typical halo masses, in the range $logM_h[h^{-1}\mathrm{M}_\odot] \sim 12.5 - 13.5$. These results have usually been interpreted as a possible sign of alternative triggering mechanisms at play (Fanidakis et al. 2011).

However, great attention must be paid in interpreting these observational results. For example, the relatively small number of AGN, typically around a few percent of the whole galaxy population at z<1, requires especially in deep surveys the use of large AGN samples covering wide ranges of redshift, luminosity and host galaxy properties to gather statistically significant samples. This in turns renders the comparison among different data-sets non-trivial.

The halo occupation distribution (HOD) formalism (Cooray & Sheth 2002; Berlind et al. 2003; Cappelluti et al. 2012) allows to extract from the 2PCF the full distribution of host halo masses for a given sample of AGN. The halo model in fact constraints the AGN HOD function P(N|M_h), which provides the probability distribution for an halo of mass M_h to host a number N of AGN above a given luminosity. Only recently a number of observational studies have begun to focus on the AGN HOD, although still facing uncertainties due the degeneracy in the shape and normalization of the HOD (e.g, Shen et al. 2013).

Given the uncertain observational situation, a valuable complimentary way to effectively probe the different interpretations concerning clustering analysis, is to rely on a comprehensive cosmological model for galaxy formation. For instance, implementing various physical mechanisms for triggering AGN activity in a semi analytic model (SAM) for galaxy formation (see Baugh 2006 for a review), it is possible to compare the predicted $P(N|M_h)$ of each different model with a wide range of different AGN 2PCF and HOD measurements, in order to narrow down the efficiency of each separate AGN triggering mechanism included in the SAM.

In Menci et al. (2014) and Gatti et al. (2015) we included in an advanced SAM for galaxy formation two different analytic prescriptions for triggering AGN activity in galaxies. We first considered AGN activity triggered by disk instabilities (DI scenario) in isolated galaxies, and, separately, the triggering induced by galaxy interactions (major mergers, minor mergers and fly-by events, IT scenario). The analytic prescriptions included in the SAM to describe each physical process are based on hydrodynamical simulations, thus offering a solid background for describing accretion onto the central SMBH.

Relying on this framework, the aim of this paper is to investigate the imprint left by each separate triggering process (IT and DI modes) on the clustering strength of the AGN population, both on small and large scales and at different redshift and luminosity. The final goal is to highlight key features in the clustering properties of the two modes that might constitute robust probes to pin down the dominant SMBH fueling mechanism.

The paper is organized as follows. In Sect. 2, we briefly describe our SAM and the two AGN triggering mechanisms considered. In Sect. 3, we review the HOD formalism and the theoretical model used to obtain the 2PCF. In Sect. 4 and 5, we present our main results concerning the clustering properties of the AGN population as predicted by our two modes and we compare with a wide range of observational constraints (both AGN HOD and 2PCF measurements). We discuss our results in Sect. 6 and summarize in Sect. 7. Throughout the paper we assume standard ΛCDM cosmology, with $\Omega_M = 0.3$,$\Omega_\Lambda = 0.7$, $\Omega_b = 0.045$, $\sigma_8 = 0.8$, to make contact with the one adopted in most of the observations we will be comparing our models to.

2 SEMI-ANALYTIC MODEL

2.1 Evolving dark matter halos and galaxies in the model.

Our analysis relies on the semi analytic model (SAM) described in Menci et al. (2006, 2008, see Menci et al. 2014 for the latest update), which connects the cosmological evolution of the underlying dark matter halos with the processes involving their baryonic content such as gas cooling, star formation, supernova feedback, and chemical enrichment.

An accurate Monte Carlo method tested against N-body simulations is used to generate the merging trees of dark matter halos following the extended Press & Schechter formalism (Bond et al. 1991; Lacey & Cole 1993), ultimately providing the merging rates of dark matter halos. As cosmic time proceeds, smaller halos are included in larger ones as satellites. A satellite might either merge with another satellite during a binary aggregation or fall into the centre as a result of dynamical friction, contributing to increasing the mass content of the central dominant galaxy. The typical central-satellite merging timescales increase over cosmic time, thus inevitably increasing the number of satellites as the host halos scale up from groups to clusters (Menci et al. 2006).

The baryonic processes taking place in each dark matter halo are computed as follows: for a given galactic halo of mass M_h, at the moment of its formation we assign to the hot phase an initial amount $M_h\Omega_b/\Omega_M$ of gas at the virial temperature. As the cosmic time proceeds, an increasing fraction of the gas in the hot phase progressively cools and settles into a rotationally supported disk with mass M_c, disk radius R_d and disk circular velocity V_d computed as in Mo et al. (1998).

The cooled gas M_c is gradually converted into stars at a rate $\dot{m}_* \propto M_c/t_d$. The consequent stellar feedback returns a fraction of the cooled gas to the hot gas phase at the virial temperature of the halo. An additional channel of star formation implemented in the model is provided by the starburst following the triggering of AGN activity (see below).

2.2 AGN triggering

Two different AGN feeding modes are implemented in our SAM:

i) IT mode. The triggering of the AGN activity is provided

by galaxy interactions (major mergers, minor mergers and fly-by events).

ii) DI mode. The accretion onto the central SMBH occurs due to disk instabilities, where the trigger is provided by the break of the axial symmetry in the distribution of the galactic cold gas.

DI and IT modes have been included and operate in the SAM separately. The full properties of the AGN population are always determined only *by one* of the two feeding modes. In the following, we give a basic descriptions for both IT and DI models.

2.2.1 IT mode

In a galactic halo with given circular velocity v_c inside a host halo with circular velocity V, galaxy interactions occur at a rate

$$\tau_r^{-1} = n_T(V)\,\Sigma(r_t, v_c, V)\,V_{rel}(V), \quad (1)$$

where $n_T = 3N_T/4\pi R_{vir}^3$ is the number density of galaxies in the host halo, V_{rel} the relative velocity between galaxies, and Σ the cross section for such encounters, which is given by Saslaw (1985) in terms of the tidal radius r_t associated with a galaxy with given circular velocity v_c Menci et al. (2004). Any kind of interaction destabilizes a fraction f of cold gas in the galactic disk; the fraction can be expressed in terms of the variation Δj of the specific angular momentum $j \approx GM/V_d$ of the gas as (Menci et al. 2004)

$$f \approx \frac{1}{2}\left|\frac{\Delta j}{j}\right| = \frac{1}{2}\left\langle \frac{M'}{M}\,\frac{R_d}{b}\,\frac{V_d}{V_{rel}}\right\rangle, \quad (2)$$

where b is the impact parameter, evaluated as the greater of the radius R_d and the average distance of the galaxies in the halo, M' is the mass of the partner galaxy in the interaction, and the average runs over the probability of finding such a galaxy in the same halo where the galaxy with mass M is located. We assume that in each interactions 1/4 of the destabilized fraction f feeds the central BH, while the remaining feeds the circumnuclear starbursts (Sanders & Mirabel 1996). Hence, the BH accretion rate is equal to

$$\frac{dM_{BH}}{dt} = \frac{1}{4}\frac{f\,M_c}{\tau_b}, \quad (3)$$

with $\tau_b = r_d/v_d$ the timescale for the AGN to shine.

2.2.2 DI mode

In the DI scenario, disk instability arises in galaxies whose disk mass exceeds a given critical value

$$M_{crit} = \frac{v_{max}^2 R_d}{G\epsilon}, \quad (4)$$

where v_{max} is the maximum circular velocity, R_d the scale length of the disk, and $\epsilon \sim 0.5 - 0.75$ a parameter calibrated against simulations (we set its value to be $\epsilon = 0.75$, in order to maximize the efficiency of the DI scenario). The above critical mass is provided by Efstathiou et al. (1982) on the basis of N-body simulations. At each time step of the simulation, we compute the critical mass competing to each galaxy following Eq. 4. If the criterion is satisfied, then we assume the disk becomes unstable driving a mass inflow onto the central SMBH and a circumnuclear starburst. The mass inflow is computed according to the model proposed by Hopkins & Quataert (2011) and is equal to:

$$\dot{M}_{BH} \approx \frac{\alpha\, f_d^{4/3}}{1 + 2.5\, f_d^{-4/3}(1 + f_0/f_{gas})} \times \left(\frac{M_{BH}}{10^8 M_\odot}\right)^{1/6} \left(\frac{M_d(R_0)}{10^9 M_\odot}\right)\left(\frac{R_0}{100pc}\right)^{-3/2} M_\odot yr^{-1}, \quad (5)$$

where

$$f_0 \approx 0.2 f_d^2 \left[\frac{M_d(R_0)}{10^9 M_\odot}\right]^{-1/3} \qquad f_{gas} \equiv \frac{M_{gas}(R_0)}{M_d(R_0)}. \quad (6)$$

Here M_{BH} is the central black hole mass, f_d is the total disk mass fraction, M_d and M_{gas} the disk and the gas mass calculated in R_0 (we take $R_0 = 100$ pc). The constant α parametrizes several uncertainties related to some of the basic assumptions of the mass inflow model; its value is not completely freely tunable, but physically admissible values are in the range $\alpha = 2 - 10$ (see Menci et al. 2014 and Gatti et al. 2015 for further details). A higher normalization ($\alpha = 10$) roughly corresponds to slightly higher AGN luminosity and shorter duty cycle, since there is a faster gas consumption and a faster stabilization of the disk. The opposite is true for lower normalizations.

In what follows, we will show for the DI scenario three different predictions, corresponding to the cases $\alpha = 2, 5$ and 10, so as to span all the reasonable values of the normalization of the mass inflow predicted by the model.

For both scenarios, we converted the BH mass inflows into AGN bolometric luminosity using the following equation:

$$L_{AGN} = \eta\, c^2\, \dot{M}_{BH} \quad (7)$$

We adopted an energy-conversion efficiency $\eta = 0.1$ (Yu & Tremaine 2002; Marconi et al. 2004; Shankar et al. 2004, 2009). The luminosities in the UV and in the X-ray bands were computed from the above expression using the bolometric correction given in Marconi et al. (2004).

In Menci et al. (2014) and Gatti et al. (2015) we already constrained the regimes of effectiveness of the two mechanisms by comparing them with a wide range of different properties concerning the AGN population (AGN luminosity function, Eddington ratio distribution, Magorrian relation, etc.) and AGN host galaxies (host galaxy mass function, colors magnitude diagram, $SSFR - M_*$ relation, etc.). While our IT scenario provided a quite good match to all the observational constraints we compared with, DIs were effective mainly in triggering moderately luminous ($L \sim L_{knee}$) AGN, hosted by medium sized ($M_* < 10^{11}$M$_\odot$), disky and gas rich galaxies. These ranges of validity for the DI scenario must be kept in mind in the next sections when comparing with clustering measurements.

We stress that the results in this work do not heavily rely on the exact implementation of these two processes in our SAM, nor on the exact parameterization/modelling adopted for evolving the galaxies within their host dark matter haloes (Sect. 2.1). In fact, the frequency and type of IT mainly depend on the dark matter merger rates, dynamical friction and encounter timescales, which are common features in every galaxy evolution model based on a ΛCDM cosmology. The DIs are instead "in-situ" processes, mainly controlled by the disk instability criterion of eq. 4. While eq. 4 is clearly a condition tightly linked to the specific features of the SAM (scale radius evolution, maximum circular velocity), we show

that our main results are broadly preserved irrespective of the exact threshold chosen for the disk instability. Moreover, a number of comparison studies have shown that our SAM is quite "typical", producing galactic outputs at all epochs in line with several other state-of-the-art SAMs (e.g., Gruppioni et al. 2015).

3 PROBING AGN CLUSTERING PROPERTIES: AGN MOF AND 2PCF CALCULATION

To investigate the clustering properties of the AGN population we make use of two key probes: the mean AGN occupation function (MOF) $N(M_h)$ and the AGN 2-point correlation function (2PCF) $\xi(r)$.

Our SAM, by accounting for the evolution of the AGN population along with the evolution of the dark matter density field, directly provides the AGN MOF for each timestep of the simulation. As a standard practice we express the AGN MOF for the DI and IT modes as the sum of a central and a satellite component $\langle N(M_h)\rangle = \langle N(M_h)\rangle_{cen} + \langle N(M_h)\rangle_{sat}$.

Concerning the AGN 2PCF, we compute it from the predicted AGN MOF through the use of the halo model formalism (Kauffmann et al. 1997; Cooray & Sheth 2002; Tinker et al. 2005; Zheng & Weinberg 2007). The halo model assumes that the two-point correlation function $\xi(r)$ can be faithfully described as the sum of two contributions: the 1-halo term $\xi_{1-h}(r)$, mainly due to the contribution of AGN residing in the same halo, and the 2-halo term $\xi_{2-h}(r)$, due to the correlation of objects residing in different halos. Both terms can be obtained from the AGN MOF once having specified the halo mass function $n(M_h)$ (Press & Schechter 1974; Sheth & Tormen 1999) and the halo bias factor $b(M_h)$ at a specific redshift. More details on the halo model and on how we compute the 1-halo and 2-halo terms are given in Appendix A.

A point that is important to stress is that both the AGN MOF and the 2PCF obtained from our SAM are not affected by any evident degeneracy concerning their shape and normalization. In basic HOD modelling instead, the AGN MOF is usually inferred indirectly from clustering measurements: once having assumed a parametric expression for $\langle N(M_h)\rangle$, the 2PCF is used to constrain the parameters of the AGN mean occupation function. This indirect approach is however limited by the inevitable degree of degeneracy in the different parameterizations of the input MOF that can account for the measured the 2PCF (e.g., Shen et al. 2013).

Our direct approach conversely starts from the predicted AGN mean occupation functions provided by our SAM, which in turn yields, within the HOD formalism, a unique expression for the 1-halo and 2-halo terms of the AGN 2PCF.

4 RESULTS: GENERAL TRENDS

In this section we present the results concerning the clustering properties of the IT and DI scenarios. Before focusing on a detailed comparison with a number of AGN MOF and 2PCF measurements, we discuss some important, general features of the clustering properties of our two models.

4.1 AGN duty cycle

As a first check, fig. 1 shows the AGN duty cycle for the two scenarios as a function of dark matter host halo mass and AGN bolometric luminosity. This plot is useful to pin down the luminosity

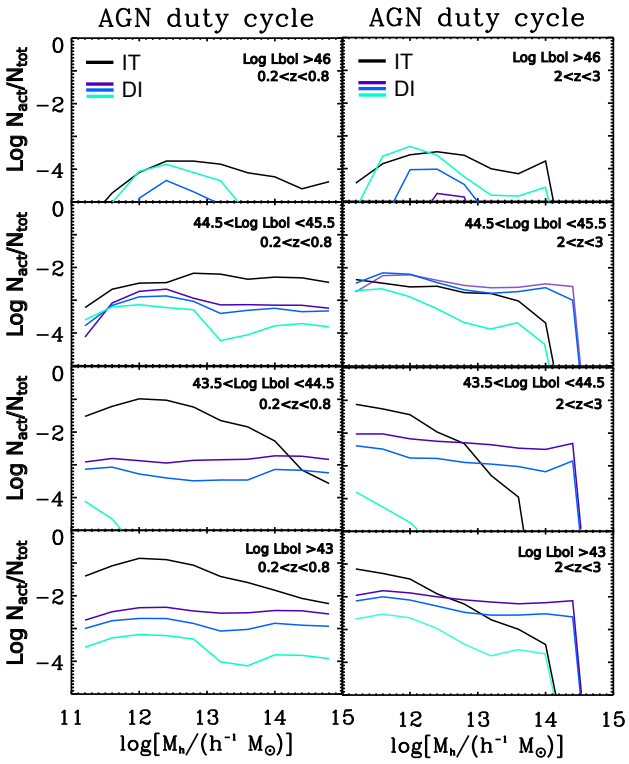

Figure 1. AGN duty cycle for the DI and IT scenarios as a function of AGN bolometric luminosity and dark matter host halo mass, computed at redshift $0.2 < z < 0.8$ and $2 < z < 3$. Only galaxies with $M_* > 10^9 M_\odot$ have been considered. The predictions of our model are represented by continuous lines: black line for the IT scenario, light blue, blue and purple for the DI scenario. Light-blue represents the prediction with the highest value of the normalization of the inflow (see Sect. 2.2), blue for the intermediate value, purple for the lowest value.

intervals and the typical environments where DI and IT are most efficient in triggering AGN activity in galaxies. In computing the AGN duty cycle, we have taken into account galaxies with stellar mass $M_* > 10^9 M_\odot$.

At low redshift ($z \sim 0.5$), the IT scenario is in general more efficient than DIs in triggering AGN activity in galaxies, especially for low luminosity AGN ($L_{bol} \sim 44$). Conversely, at higher redshift ($z \sim 2.5$), DIs substantially increase their efficiency, due to the higher gas and disk fraction of AGN host galaxies, becoming more efficient than galaxy interactions in triggering moderately luminous AGN ($LogL_{bol} \sim 45$).

In the IT scenario the AGN duty cycle depends both on the environment and on the AGN luminosity. Luminous AGN are mainly found in dark matter halos with mass $M_H \sim 10^{12} h^{-1} M_\odot$, while the AGN duty cycle flattens for moderately luminous AGN ($L_{bol} \sim 45$). Low-luminosity AGN, which dominate by number the total AGN population, are again characterized by a substantial peak around $M_H \sim 10^{12} h^{-1} M_\odot$. Galaxy interactions are indeed favored in group environments, due to a high density of galaxies with low relative velocity (lower with respect to massive clusters). This differs substantially from the prediction of the DI scenario. Aside for high luminosity AGN, the AGN duty cycle is almost flat, both at low and high redshift. As expected, being "in-situ" processes, DIs are in fact not necessarily linked to the large-scale structure environment.

Fig. 2 shows the AGN duty cycle as a function of host galaxy stellar mass instead of dark matter halo mass. Our predictions are

here compared with data from Aird et al. (2012) and Bongiorno et al. (2012).

First, we note that all the predictions for the IT scenario for the different luminosity/redshift bins are broadly characterized by the same shape, differing only in their normalization. This feature, as also noted by Bongiorno et al. (2012), indicates that this scenario must be characterized by a broad Eddington ratio distribution, which is what we showed in Menci et al. (2014) for the IT scenario. Broad Eddington distributions naturally allow for the more massive systems to be active at different modes thus increasing their duty cycle (see also, e.g., Shankar et al. 2010, 2013, and references therein). A narrower distribution, instead, would force the most luminous AGN to be preferentially linked to the most massive, less numerous SMBH and host dark matter halos.

The DI scenario, on the contrary, does show some luminosity dependence. The most luminous AGN are preferentially hosted by the most massive galaxies, with the distribution spreading towards lower stellar masses for lower luminosities. This feature follows from an underlying tighter Eddington ratio distribution characterizing the DI scenario, a trend already noted in Menci et al. (2014).

Some relevant discrepancies between our predictions and observational data need to be discussed at this point. First of all, we note that the DIs fall short in triggering AGN activity in massive galaxy hosts: regardless of the luminosity and redshift range, the duty cycle drops for galaxies with mass $M_* > 10^{11}\mathrm{M}_\odot$. In brief, as outlined by Gatti et al. (2015), disk instabilities tend to be disfavored by low gas and disk fractions, a typical condition for massive galaxies.

Second, there is substantial over production of faint AGN ($42 < LogL_X < 43$) at $z < 1$ for the IT scenario, especially in low-mass hosts. Even if this might partially be due to an underestimate in the data completeness correction for low luminosity AGN, we expect the IT scenario to over-produce faint AGN, owing to the well known excess of small objects produced by SAMs. However, this should little affect the main results of this paper, since the majority of the data we will be comparing our models to hardly ever extend to such low luminosity/low host stellar mass sample.

Finally, a more severe discrepancy occurs at high redshift with respect to data from Bongiorno et al. (2012). Their data imply a strong redshift evolution of the AGN duty cycle ($\propto (1+z)^4$), which is not reproduced by our predictions, though it is broadly consistent with some continuity equation models (e.g., Shankar et al. 2013). From the point of view of our SAM, we can have basically two different explanations: 1) the IT and DI models do not produce enough moderate-to-high luminosity AGN at such redshifts; 2) there is an incorrect correspondence between the AGN luminosity and galaxy stellar mass.

However, our models show a pretty good match with the AGN luminosity function at redshift $1 < z < 2$ (especially in the IT scenario). Even accounting for the uncertainties in the LF measurements, this cannot totally explain the one order of magnitude discrepancy shown by the AGN duty cycle in fig. 2. It is possible that the AGN duty cycle in the most massive bin might be affected by statistical fluctuations owing to the low abundance of massive hosts. At face value, the most relevant point might concern the correspondence between the AGN luminosity and galaxy stellar mass.

It is also important to stress that observational biases and completeness correction might have a role here, affecting the estimate of the AGN duty cycle and possibly contributing to the discrepancy with our SAM. We note that the data from Aird et al. (2012) and Bongiorno et al. (2012) are not in perfect agreement with each other (if we consider overlapping redshift bins), with our SAM best reproducing the data from Aird et al. (2012). This tension between the two data sets might depend, for instance, on the AGN host galaxy mass estimate, which is related to the technique used to perform the SED fitting. In this respect, Bongiorno et al. (2012) noted that fitting the optical SED with a galaxy+AGN template produces masses from 10 times smaller to 6 times higher than the estimates obtained using a galaxy template only (which is the case of Aird et al. 2012).

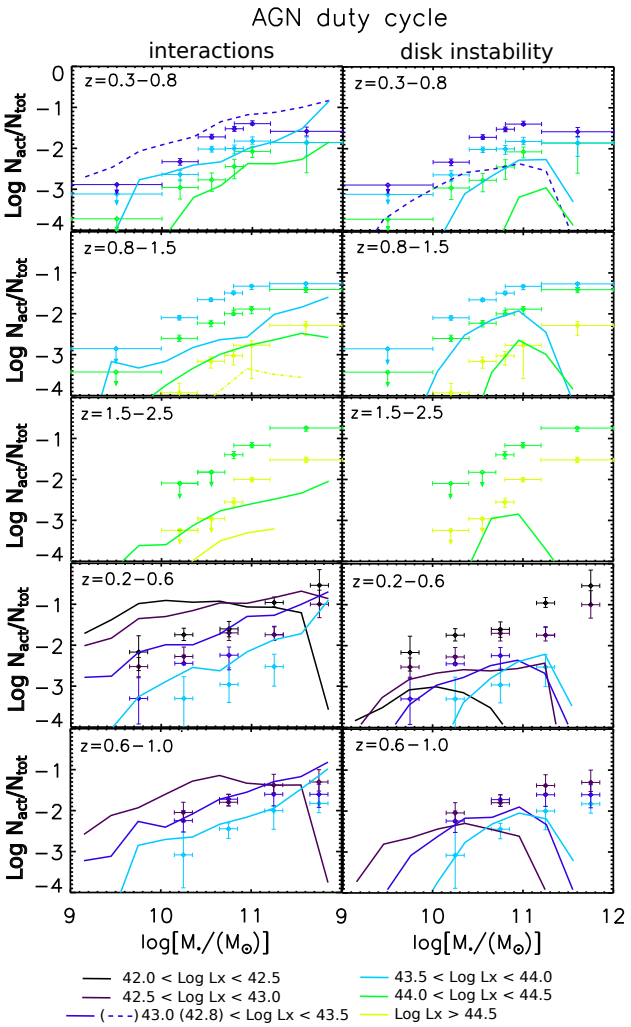

Figure 2. AGN duty cycle for the DI and IT scenarios as a function of AGN bolometric luminosity and host galaxy stellar mass. The three upper rows show the comparison with data from Bongiorno et al. (2012), while in the two lower ones we compare with data from Aird et al. (2012). For the DI scenario, only the prediction with $\alpha = 2$ is shown.

Assuming that the discrepancy between our predictions and data at high redshift is a true discrepancy, we note that if the models are failing in reproducing the normalization of the AGN duty cycle for every stellar mass, this should only affect the normalization of the AGN MOF and not the AGN 2PCF, if the relative probability of triggering centrals and satellites remains unaltered. Conversely, if we are assigning at some fixed L_{bol} a lower (higher) stellar mass, we will under (over) predict the average AGN bias factor.

4.2 Redshift and luminosity dependence of AGN clustering

A second preliminary investigation concerns any redshift and luminosity dependence of predicted clustering of AGN. Several authors

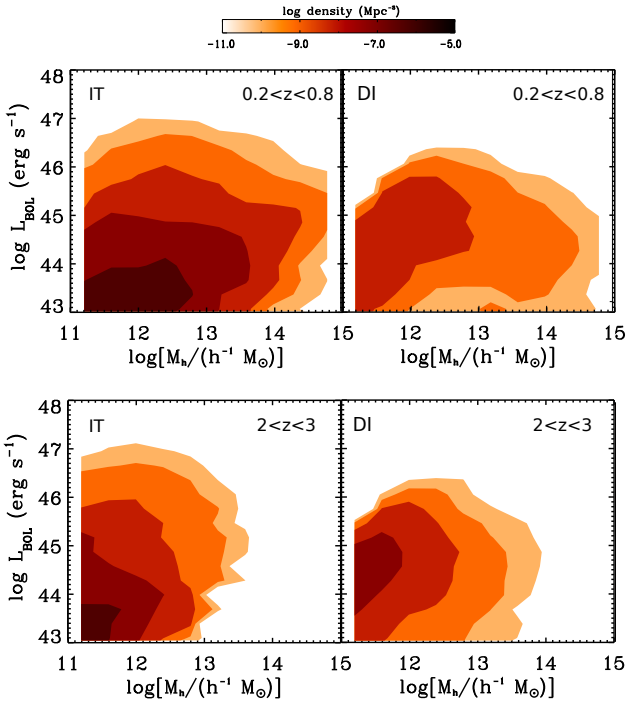

Figure 3. Contour plots representing the number density of AGN as a function of host halo mass and AGN bolometric luminosity, for two different redshift bins ($0.2 < z < 0.8$ and $2 < z < 3$). Both the predictions for the IT and DI scenario are shown (left and right panels respectively). As for the DI scenario, only the prediction with normalization $\alpha = 0.5$ is considered. No additional cut in the AGN host galaxy properties has been considered.

have investigated the luminosity and redshift evolution of clustering measurements. We summarize the observational results obtained so far in Appendix B.

Fig. 3 provides some insights into any redshift and luminosity dependence of AGN clustering for the DI and IT scenario. The contour plots represent the number density of AGN as a function of host halo mass and bolometric luminosity, for two different redshift bins.

At low redshift, fig. 3 shows that luminous AGN $LogL_{bol} > 46$ inhabit mainly halos with mass $\sim 10^{12} - 10^{13}\mathrm{M}_{\odot}$ for both the IT and DI scenarios (even if DIs do not trigger the most luminous AGN with $LogL_{bol} \sim 47$). As we consider intermediate luminosities ($LogL_{bol} \sim 44 - 45$), the distribution gradually spreads over the full range of halo masses; this is particularly true for the IT scenario, while for the DI scenario the spreading is less pronounced (see the levels of the countour plot, indicating that the majority of DI AGN inhabit low mass environments). Finally, for low luminosity AGN ($LogL_{bol} \sim 43 - 44$), the distribution becomes slightly steeper towards lower halo masses.

This non-linear behavior in the number densities of active galaxies can be explained as follows. Luminous AGN are naturally found in halos with mass $\sim 10^{12} - 10^{13}\mathrm{M}_{\odot}$ because the most luminous AGN necessarily require large gas reservoirs and massive BHs.

For the IT scenario, luminous AGN are triggered by strong interactions, which are more common in less massive environments than in clusters, due to a higher relative velocity between galaxies. For the DI scenario the SMBH mass inflow is maximized by the presence of an unstable, massive and gas rich disk (see eq. 5), which cannot be found in massive environments Moderately luminous AGN are less constrained by the above-mentioned requirements and naturally reside in a wide range of dark matter halos. Ultimately, the slight increase towards low halo masses for low luminosity AGN might be due to the tendency of low mass SMBHs to reside on average in less massive dark matter halos.

As for the high redshift ($z \sim 2.5$) bin, the most relevant difference with respect to the low redshift case is that all AGN activity is moved towards less massive halos. In short, structures with mass greater than $M_h > 10^{13}$ become significantly rarer, relegating active galaxies to live mainly in less massive environments. This plot alone would suggest a non-negligible redshift evolution of the AGN clustering, calling into question the use of wide redshift interval to compute the AGN 2PCF.

In the standard prediction obtained accounting for all the AGN residing in $M_h > 10^{11}h^{-1}\mathrm{M}_{\odot}$, we note that the average bias factor (i.e., the bias factor computed over the full luminosity interval) is very similar for the two scenarios, being dominated by the less luminous AGN and averaging at around $b \sim 1.1$, roughly corresponding to $M_h \sim 10^{12}h^{-1}\mathrm{M}_{\odot}$ (fig. 4). Luminous AGN are associated with a slightly higher bias factor with respect to faint AGN, corresponding to dark matter halos as massive as $M_h \sim 10^{12.5}h^{-1}\mathrm{M}_{\odot}$, but in general, no strong evidence for luminosity dependence is observed. At redshift $z \sim 2.5$, the two scenarios are again characterized by similar average bias factors ($b \sim 2.3$, corresponding to $M_h \sim 10^{11.5}h^{-1}\mathrm{M}_{\odot}$), with the most luminous AGN residing again in slightly more massive dark matter halos ($M_h \sim 10^{11.9}h^{-1}\mathrm{M}_{\odot}$). With respect to the low redshift case, a consistent evolution towards lower dark matter halo mass is observed, for every luminosity bin.

The analysis of the bias factor alone as shown in fig. 4, might not be a sufficient discriminator for AGN triggering mechanisms, being the differences relatively small, with also relatively weak luminosity dependence.

Nevertheless, there is an important point that needs to be stressed. In fig. 3 and 4 we have not made any particular cut in the properties of the AGN host galaxy population, simply considering AGN residing in dark matter halos more massive than $M_h > 10^{11}h^{-1}\mathrm{M}_{\odot}$. However, any additional selection in the host galaxy properties might alter the distribution, affecting the implied bias factor. Among all, the major effect might be represented by the clustering dependence on the host galaxy stellar mass, since it is known to correlate to the dark matter halo mass (Vale & Ostriker 2004; Shankar et al. 2006; Moster et al. 2013; Shankar et al. 2014).

Fig. 4 for example shows that considering only galaxies with $M_* > 10^{10.5}\mathrm{M}_{\odot}$ considerably alters the bias factor distributions. Irrespective of the exact model, the overall bias as a function of bolometric luminosity in fact increases in normalization and flattens out. This proves that the underlying AGN light curve (e.g., Lidz et al. 2006) is not the only responsible for shaping the bias-L_{bol} relation. Particularly, at low redshift the average bias factor corresponds to halos with $M_h \sim 10^{12.5}h^{-1}\mathrm{M}_{\odot}$, while at high redshift we have $M_h \sim 10^{12\cdot}h^{-1}\mathrm{M}_{\odot}$. Since high redshift observations are generally biased towards bright hosts with high stellar mass, this (often implicit) cut in host galaxy stellar mass might hide a possible intrinsic redshift evolution in the bias factor.

4.3 AGN satellite fraction

Another general feature of our DI and IT models that can be investigated is the AGN satellite fraction f_{sat}, i.e. the fraction of AGN that reside in satellite galaxies with respect to the total AGN population.

From an observational point of view, clustering measurements constrain the AGN satellite fraction mainly from small-scale clus-

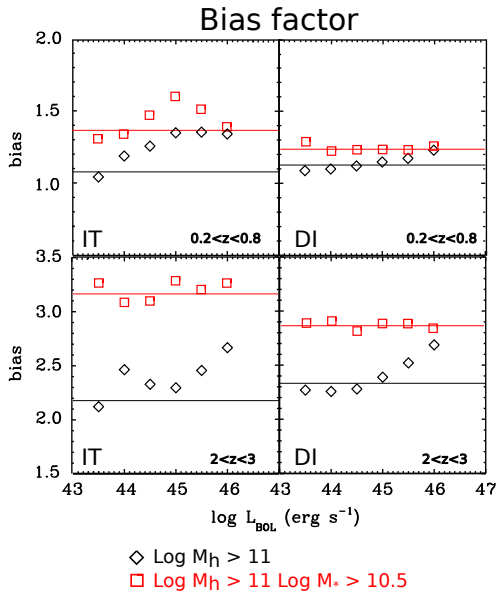

Figure 4. Bias factor of the AGN population for the DI and IT scenarios, as a function of redshift and AGN bolometric luminosity. Black diamonds refer to the bias factor computed considering AGN residing in halos with mass $M_h > 10^{11}h^{-1}\mathrm{M}_\odot$; red squares represent the bias factor computed considering the additional cut in the host galaxy stellar mass of $M_* > 10^{10.5}\mathrm{M}_\odot$. Horizontal lines represent the average bias factor over the full luminosity range.

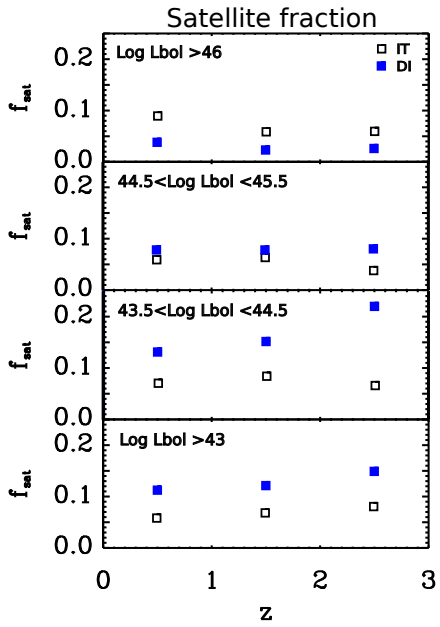

Figure 5. AGN satellite fraction, defined as the fraction of AGN in satellite galaxies, as a function of redshift and AGN bolometric luminosity. In computing the satellite fraction, AGN residing in halos with mass $M_h > 10^{11}h^{-1}\mathrm{M}_\odot$ have been considered. The predictions for the DI scenario are represented by filled blue squares, while those for the IT scenario by black empty squares. For the DI scenario, only the prediction with normalization $\alpha = 5$ is shown.

tering, with an associated systematic uncertainty broadly related to the exact parametric form adopted for the input MOF. Previous observational estimates both at low (z ∼ 0.5) and intermediate redshift (∼ 1.5) have derived a satellite fraction usually in the range $f_{sat} \sim 0.01 - 0.1$, with $f_{sat} \sim 10\%$ often considered an upper limit (Starikova et al. 2011; Richardson et al. 2013; Shen et al. 2013; Kayo & Oguri 2012), though Leauthaud et al. 2015 claim a satellite fraction as high as $f_{sat} \sim 18\%$.

Fig. 5 shows the AGN satellite fraction f_{sat} as predicted by our models, at different redshift and for different luminosity cuts. In general, the AGN satellite fraction does not show any clear evolutionary trend with redshift, with its value oscillating in the range 0.05 ∼ 0.15. Galaxy interactions are characterized on average by a slightly lower satellite fraction ($f_{sat} \sim 0.05 - 0.1$) with respect to the DI scenario ($f_{sat} \sim 0.075 - 0.15$), except for the highest luminosity bin ($LogL_{bol} > 46$). The difference between the two models becomes even more evident when considering the satellite fraction as a function of the dark matter host halo mass (fig. 6). Especially in the most massive hosts (groups and clusters), the fraction strongly increases and saturates to unity for the DI scenario, indicating that no AGN is triggered in central galaxies, while in the IT scenario the increment is not as pronounced and the fraction settles around lower values.

The low f_{sat} in the IT scenario is induced by a very low probability of triggering satellite galaxies (the cross section for satellite interactions is small, see for instance Angulo et al. 2009), and the very high probability of triggering centrals. Conversely in the DI scenario central galaxies are generally less favored: at a fixed halo mass, central galaxies are more massive and with lower gas fraction with respect to satellites, leading to a higher probability of triggering satellites rather than centrals. We stress that while the exact value might be susceptible to the details of our modeling, the general prediction of a high satellite fraction for the DI scenario, whose main requirements are high disk and gas fractions, should be considered robust (see Sect. 6 for a further discussion).

A first comparison with data from Martini et al. (2009) and Pentericci et al. (2013) (fig. 6 lower panels) seems to indicate that the IT scenario might not trigger enough intermediate-to-low luminosity AGN in satellite galaxies in massive environments (groups and clusters) at $z \lesssim 1$. This could suggest that other mechanisms besides our IT scenario might contribute to the triggering of satellite AGN in such environments. We caution, however, that the comparison in fig. 6 should not be assumed as a conclusive test for the absolute predominance of the DI mode in triggering satellite AGN. The fraction f_{sat}, indeed, provides only the relative number of satellite AGN, not the absolute abundance, and the apparent better match of the DI mode might be simply due to a shortage of central active galaxies. We will better investigate the abundance of central and satellite AGN predicted by our models in the next sections.

5 RESULTS: COMPARISON WITH OBSERVATIONS

We present here the comparison between the outputs of our SAM concerning the DI and IT mode, and several 2PCF and MOF measurements.

The AGN samples we compare with are characterized by different redshift and luminosity ranges, and are extracted from both bright quasar optical surveys and moderately luminous AGN X-ray surveys. To broadly take into account the observational selections relative to the different types of surveys, we decided to make use of an observational absorption function (Ueda et al. 2014). The latter provides the fraction of AGN with a certain column density N_H as a function of AGN luminosity and redshift. When comparing with measurements from bright quasar optical surveys, for exam-

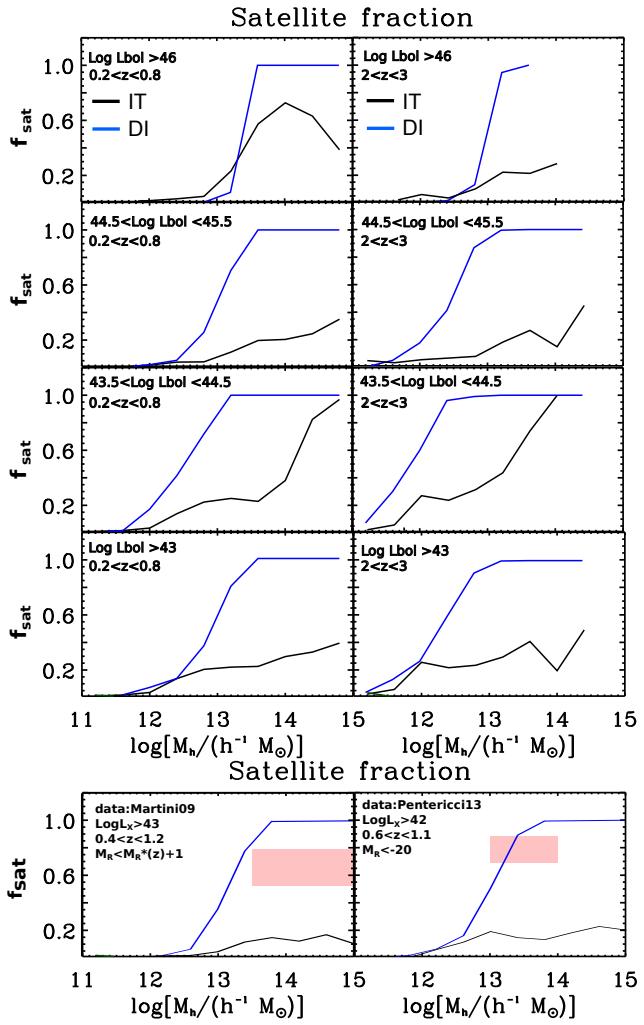

Figure 6. *Upper panels:*AGN satellite fraction as predicted by our models as a function of AGN luminosity and dark matter halo mass, for two redshift bins. For the DI scenario, only the prediction with normalization $\alpha = 5$ is shown. *Lower panels:* same as upper panels, but compared with data from Martini et al. (2009) and Pentericci et al. (2013). The observed fraction (red box) has been obtained from the AGN radial distribution expressed in R/R_{200}, considering as satellites all the AGN not belonging to the innermost radial bin. The box represents the 1-σ interval computed with the low number statistics estimator by Gehrels (1986).

ple, we filtered the SAM mock AGN catalogs through our adopted absorption function to select only unobscured AGN with column density $N_H < 10^{22} cm^{-2}$. On the other hand, we excluded AGN with $N_H > 10^{24} cm^{-2}$ (CTK population) when we compared with measurements from X-ray surveys. We note however that correcting for absorption has a little impact on the exact shape of the AGN MOF predicted by our models while it mainly influences the normalization.

5.1 Comparison with AGN MOF from 2PCF measurements

First, we compare with two AGN MOF "indirect" measurements, that is, MOF obtained from clustering measurements. These AGN MOF have been obtained by the authors from the observed AGN 2PCF using the halo model framework: particularly, once having fixed a parametric expression for the AGN MOF, a Markov Chain Monte Carlo modeling of the AGN 2PCF is performed so as to probe the parameter space of the input AGN MOF. These two AGN MOF measurements from Richardson et al. (2012) and Shen et al. (2013) are shown in fig. 7, along with the predictions of our model.

In comparing our predictions with data, all the luminosity and redshift cuts concerning the different samples have been taken into account. In particular: a) we accounted for the redshift range spanned by the sample; b) in case of optical surveys, we selected AGN converting the flux limit of the survey in the i band into a limit on the AGN bolometric luminosity (following Richards et al. 2006); c) for X-ray surveys, AGN have been selected according to their flux in the soft or hard X-ray band (obtained using the bolometric corrections of Marconi et al. 2004) and the limiting flux of the survey; d) if specified in the reference paper, we also applied an additional cut on the host galaxy magnitude in the i band, so as to reproduce the selection bias related to the need of spectroscopic redshift.We provide in Appendix C a more accurate description of the different reference data sets considered in this work.

The comparison in fig. 7 broadly indicates that while the predictions for the IT scenario agree generally well with data, the predictions for the DI scenario are able to match the observational constraints only in a limited range of dark matter halo masses, depending on the sample considered.

In the three panels on the left we show the comparison with the AGN MOF from the optically selected AGN sample of Shen et al. (2013). Both the total and the central and satellite components are displayed. Their sample has an AGN median luminosity $\approx L_{knee}$, thus it probes exactly the luminosity range where the DI scenario competes with the IT one in driving the bulk of AGN activity at such redshift.

Here, the DI scenario matches the total AGN MOF only up to $10^{13.5}$ $h^{-1}M_{\odot}$, then for higher halo masses it underpredicts the number of AGN. This is mainly due to the lack of AGN in central galaxies in massive environments (central panel). Moreover, although DIs are able to trigger a discrete number of AGN in satellites, this is not enough to match the satellite AGN MOF, indicating that DIs might only contribute partially to the observed satellite AGN population.

The drop in central AGN directly follows from the results obtained in Sect. 4.1 and 4.3: DIs do not trigger AGN activity in high mass central galaxies, but rather preferentially occur in less massive satellite galaxies, with the fraction of AGN in satellite galaxies saturating to unity in massive clusters. The lack of central AGN in massive environments is present in all the comparisons we made, regardless of the luminosity and redshift cuts considered, thus it constitutes a robust feature of the DI model.

At low redshift, binary aggregations between satellite galaxies and tidal stripping contribute to disrupt galaxy disks and consume gas reservoirs, lowering the probability of triggering AGN activity by DIs.

The comparison with Richardson et al. (2012) (right panel of fig. 7) concerns an optically selected quasar sample with higher average bolometric luminosity with respect to the Shen et al. (2013) data. The comparison favors the IT scenario, while for the DI mode only the prediction with the highest normalization (and hence highest AGN luminosity) reproduces the abundance of AGN for halo masses in the range 10^{11} – $10^{12.5}$ $h^{-1}M_{\odot}$. The other two DI predictions, instead, underpredict the number of active galaxies for every dark matter halo mass. This follows from the results obtained in Menci et al. (2014), where we showed that violent major mergers rather than DIs are the most likely mechanism for triggering luminous quasars.

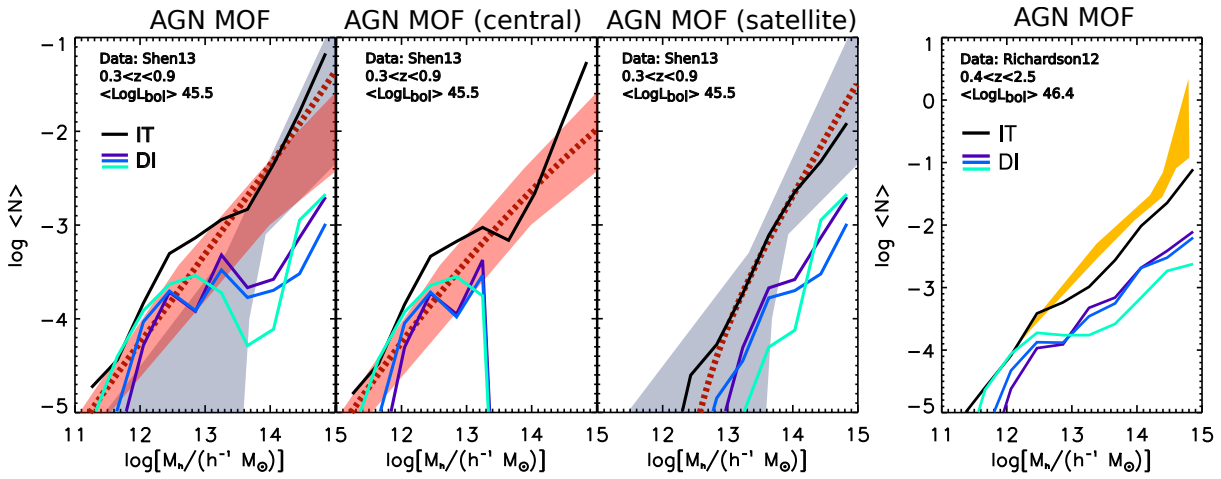

Figure 7. AGN MOF as predicted by our SAM, compared with two different AGN MOF obtained from 2PCF measurements. The predictions of our model are represented by continuous lines: black line for the IT scenario, light blue, blue and purple for the DI scenario (the color code is the same of fig. 1). *Left panels:* comparison with the AGN MOF from Shen et al. (2013). The left, central and right panels refer to the total AGN MOF and the AGN MOF of central and satellite galaxies, respectively. The red dotted lines represent the AGN MOF best fit as obtained from Shen et al. (2013); in every panel, the red-shaded region represents the 68.3% confidence interval obtained from the MCMC chain for central AGN, while the blue-shaded region is for satellite AGN. *Right panel:* AGN MOF from Richardson et al. (2012). The yellow-shaded region represents the 68.3% confidence interval for total AGN MOF as obtained from 2PCF measurements.

We remind that great attention must be paid in comparing our predictions with AGN MOF obtained from 2PCF measurements, especially when they involve wide redshift and luminosity intervals. As we stressed in Sect. 4.3, this approach basically ignores the effects of any possible redshift and luminosity evolution in the clustering strength of the AGN population.

The second main problem concerns the assumed parametric expression used to obtain the AGN MOF from 2PCF measurements. The typical choice is to assume an AGN MOF similar to the galaxy MOF, motivated by the results of hydrodynamic cosmological simulations (Di Matteo et al. 2008; Chatterjee et al. 2012): that is, a softened step function saturating to unity for central AGN and a rolling-off power law for satellite AGN. However, as pointed out by Shen et al. (2013), there is a certain degree of degeneracy in the MOF parameterizations, especially at high halo masses and in the satellite MOF, which is mainly constrained by small scale clustering (difficult to probe) and affected by the assumptions concerning the distributions of satellite AGN inside dark matter halos.

Additional probes that could more directly than the 2PCF pin down the underlying host halo distribution will be very useful to set more secure constraints on the models. We discuss some of these probes in the next section.

5.2 Comparison with AGN MOF - direct measurements and abundance matching approach

In fig. 8 we compare the predictions of our SAM with two direct AGN MOF measurements, taken from Chatterjee et al. (2013) and Allevato et al. (2012), and with the AGN MOF obtained from Leauthaud et al. (2015) using an abundance matching approach. The description concerning the samples and the selection cuts used to reproduce the observational data are given in Appendix C.2.

Similarly to the results obtained in the previous section, the IT scenario agrees well with data, while DIs generally provide a poor match.

In the comparison with the optically selected AGN sample from Chatterjee et al. (2013), only galaxy interactions are able to trigger the observed abundance of AGN in massive halos with $M_h > 10^{13.5}$ h^{-1}M$_\odot$, with DIs being disfavored as main fueling mechanism, due to the lack of AGN in central galaxies.

The other two comparisons concern relatively low luminosity, X ray-selected AGN samples at $z < 1$, therefore they are particularly useful to further test only the IT scenario, since DIs are already expected to not provide enough AGN in such luminosity range (they are most effective in triggering $L \approx L_{knee}$ AGN).

In both the comparisons with data from Allevato et al. (2012) and Leauthaud et al. (2015), our IT scenario generally provides a good match, especially for the central AGN MOF, but underpredicts the abundance of AGN in satellite galaxies, in particular when comparing with Leauthaud et al. (2015). This represents a test to what we highlighted in Sect. 4.3: the low fraction of AGN in satellite galaxies of the IT scenario seems to conflict with observational results, which favor higher AGN satellite fractions ($\sim$ 60% in the sample of Allevato et al. 2012, $\sim$ 18% in the sample from Leauthaud et al. 2015). It is possible that other mechanisms (probably other "in-situ" processes, such as stochastic accretion or cold flows) besides galaxy interactions might contribute to the triggering of AGN activity in satellite galaxies, at least for low-to-intermediate luminosity AGN.

However, it is worth noting that the lensing signal from which Leauthaud et al. (2015) obtain their AGN MOF is poorly sensitive to low satellite fractions: even if the fiducial satellite fraction inferred by the authors is equal to $f_{sat} = 18\%$, they note that reducing it to $f_{sat} = 0\%$ has only a little effect on the lensing signal, making difficult to firmly exclude values lower than the fiducial one. The low AGN satellite fraction for the IT scenario might also partially be the result of an incorrect estimate of satellite galaxies stellar mass from our SAM, since lowering the stellar mass selection cut would result into an increment of the fraction f_{sat}. Furthermore, the value of the satellite fraction inferred by Allevato et al. (2012) and Leauthaud et al. (2015) are very different from one another, suggesting that f_{sat} might be sensible to selection effects (AGN luminosity, host galaxy stellar mass, redshift) and to the environment. Even if the comparisons presented in this section represent a more

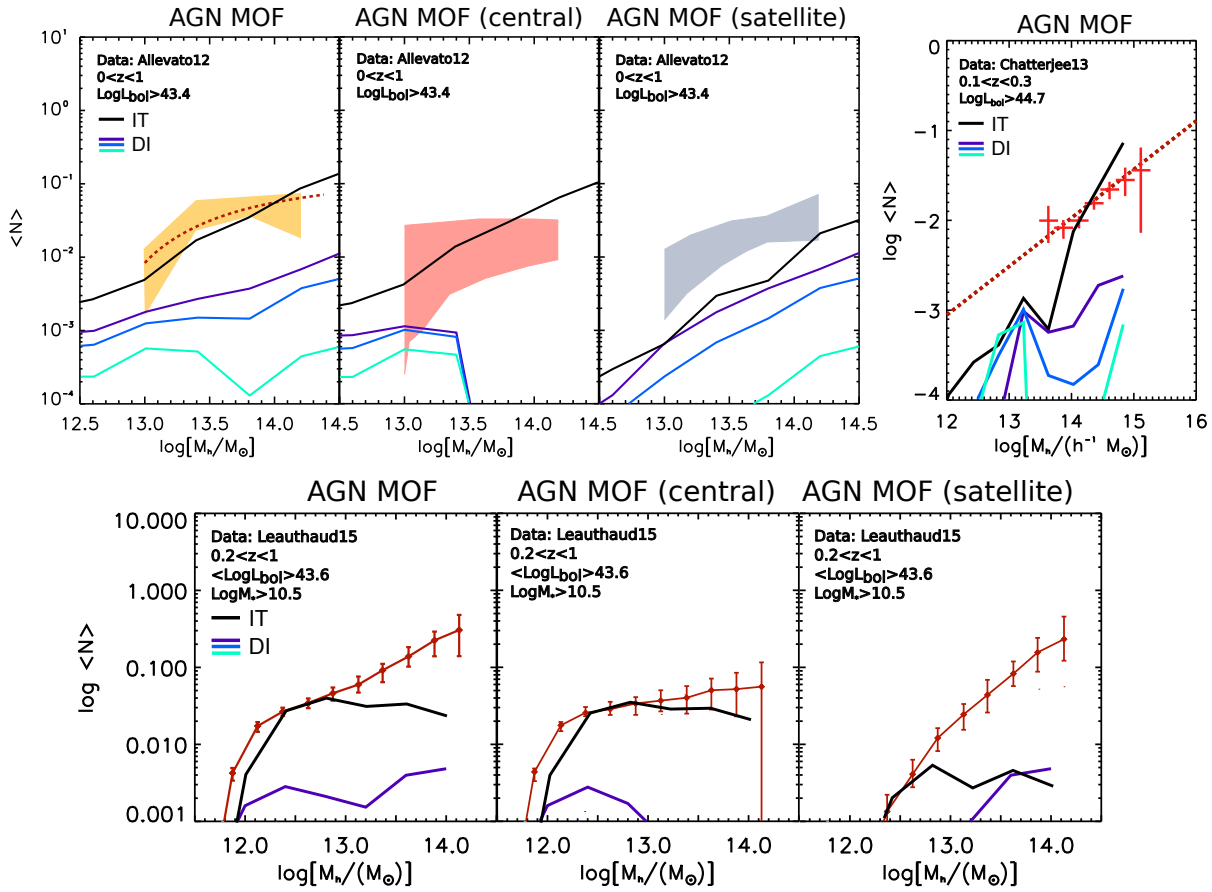

Figure 8. AGN MOF as predicted by our SAM, compared with two AGN MOF directly measured, and with one obtained using an abundance matching approach. The predictions of our model are represented by continuous lines, with the same color code of fig. 1 .*Upper-left panels:* comparison with the AGN MOF from Allevato et al. (2012). The left, central and right panels refer to the total AGN MOF and the AGN MOF of central and satellite galaxies, respectively. The red dotted lines represent the total AGN MOF best fit as obtained from Allevato et al. (2012); in every panel, the shaded region represents the 68.3% confidence interval obtained from their fit (yellow for the total AGN MOF, red for centrals, blue for satellites). *Upper-right panel:* AGN MOF from Chatterjee et al. (2012). Red crosses represent the observational data, while the red dotted line their best fit power law model. *Lower panels:* AGN MOF from Leauthaud et al. (2015); The left, central and right panels refer to the total AGN MOF and the AGN MOF of central and satellite galaxies, respectively.

reliable test of the AGN satellite MOF since data are not biased by parameterization degeneracy, more data are needed to accurately test the efficiency of our IT scenario in triggering AGN activity in satellite galaxies.

5.3 Comparison with AGN correlation function

Last, we proceed with the comparison with a number of observed AGN 2PCF at different redshifts. The AGN 2PCF provides two pieces of information: the study of the bias factor, implicit in the 2-halo term, pinpoints the average halo mass where the AGN sample resides, while the 1-halo term provides insights into the small-scale clustering, which is related to the number of AGN pairs and satellite fraction inside dark matter halos. Note that in this section we start from a model predicted MOF that *uniquely* specifies the implied 2PCF.

In fig. 9 we show the comparison of our models with four AGN auto correlation functions and one AGN-galaxy cross correlation function. The AGN-galaxy cross correlation function (Shen et al. 2013) and one AGN auto correlation function (Richardson et al. 2012) concern the same data sets relative to the AGN MOFs discussed in Sect. 5.1. The other three AGN auto correlation functions are based on a low redshift X-ray selected AGN sample from Krumpe et al. (2010), a high redshift X-ray selected AGN sample from Allevato et al. (2014), and a high redshift luminous quasars sample from Shen et al. (2007). More details about each data set we compared with are given in Appendix C.3. To obtain the 2PCF displayed in fig. 9, we made use of the bias factor and the halo mass function at the median redshift of the sample.

The data are generally reproduced quite well by our models, except for Shen et al. (2007), where we have a slight underprediction of the normalization of the 2-halo term. We note here that only the comparison with the IT scenario is shown: this sample concerns high luminosity, high redshift AGN, and we know from Menci et al. (2014) that the DI scenario is not able to trigger such AGN. The high correlation length predicted by Shen et al. (2007) measurements, together with the rareness of massive halos at high redshift, have profound implications on the quasars properties (e.g.,White et al. 2008; Bonoli et al. 2010; Shankar et al. 2010). In particular, Shen et al. (2007) data would imply a very high AGN duty cycle and AGN radiation efficiency, together with a tight $L_{bol} - M_h$ relation, which are rather extreme requirements that are difficultly met by our SAM. Given the low number of luminous quasars probed by their sample,

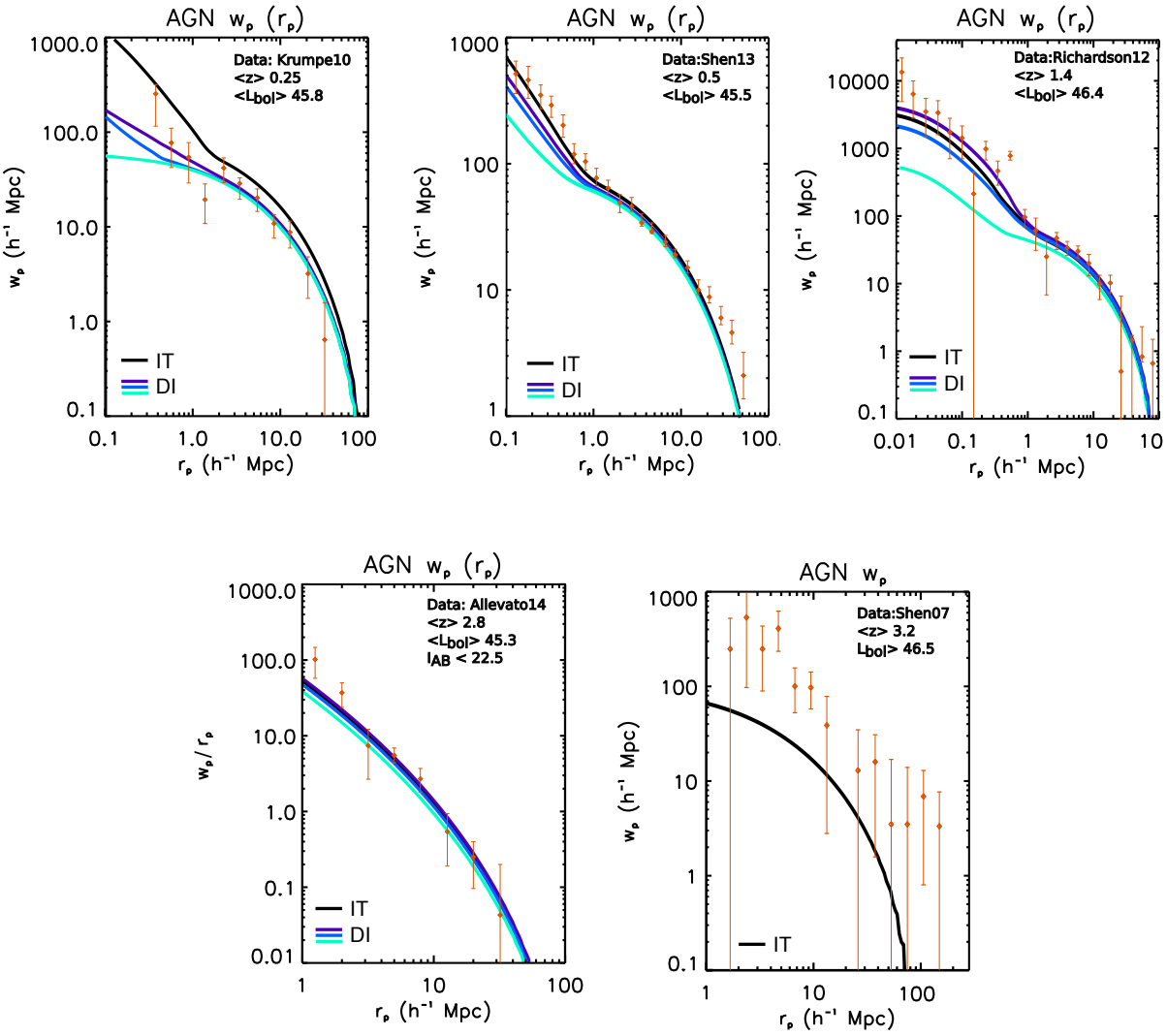

Figure 9. AGN ACF and CCF as predicted by our SAM, compared with several 2PCF measurements from Shen et al. (2007); Krumpe et al. (2010); Richardson et al. (2012, 2013); Shen et al. (2013); Chatterjee et al. (2013); Allevato et al. (2014) (see text for further details). The predictions of our model are represented by continuous lines, with the same colour code of fig. 1.

it is also possible that their correlation length is overestimated, or its statistical error underestimated.

In all the other cases, the AGN correlation functions are reproduced well by our predictions. More importantly, there is basically no appreciable difference in the 2-halo term predicted for the two scenarios in the comparisons at $z = 0.5, 1.4, 2.8$. A small difference between the two models only appears at low redshift in the comparison with Krumpe et al. (2010), with the IT scenario being characterized by a slightly higher bias factor. Even if the AGN MOF for the DI scenario always shows a drop at high halo masses, this has little impact on the average halo mass and bias factor, mainly because the more massive halos are rare, especially at high redshift, and their contribution to the normalization of the 2-halo term is almost negligible. We note that a possible drop in the central AGN MOF in massive halos might have little or no effect on the AGN 2PCF at high redshift has already been anticipated by other authors (Richardson et al. 2012; Kayo & Oguri 2012).

The results obtained in this section and in Sect. 4.2 seem to indicate that the sole analysis of the large scale clustering (i.e. bias factor) constitutes a poor constraint of the DI and IT modes considered here, especially at high redshift. Even if the AGN MOF for the two scenarios show some differences, this does not translate in an appreciable difference in the AGN 2PCF. The use of large intervals in terms of redshift and AGN luminosity to infer the AGN 2PCF further contributes to make the situation more complex.

It is also interesting to note that the AGN 2PCF measurements (as well as the AGN MOF in previous sections) we compared with concern both X-ray and optically selected AGN samples. Differences in the bias factor inferred from optical and X-ray AGN surveys have been often interpreted as a clear sign of different triggering mechanisms at play. While it is true that different triggering mechanisms might be characterized by a different clustering strength, our analysis suggests that the differences in the bias factor of surveys carried out at different wavelengths might be driven mainly by different selection cuts in terms of AGN luminosity, redshift range, host galaxy properties (e.g. stellar mass), which overcome a pos-

sible signature of different triggering mechanisms at play. In this respect, clearer selections on the host galaxy properties and smaller luminosity/redshift intervals might emphasize any difference in the clustering strength of separate SMBH feeding modes.

A similar result has been obtained by Hopkins et al. (2014): the authors compared semi-empirical models for AGN fueling based on both mergers and stochastic accretion, in which the fueling in the latter is essentially a random process arising whenever dense gas clouds reach the nucleus. They found that the stochastic fueling dominates AGN by number, though it accounts for just 10% per cent of BH mass growth at masses $10^8 M_\odot$. In total, fueling in disky hosts accounts for 30% of the total AGN luminosity density/BH mass density. They also argue that the large scale clustering is not a sensitive probes of BH fueling mechanisms, in agreement with our results.

Concerning the comparison with the small scale clustering, the situation is a little complex: small scale clustering is difficult to probe, and also the procedure we used to obtain the 1-halo term might be susceptible to the small number of AGN pairs (see also Appendix D). Nevertheless, we might expect some differences between the DI and IT scenarios. Due to the shortage of central active galaxies, DIs should be characterized on average by a lower relative number of $N_{cen}N_{sat}$ pairs, and unless they are replaced by enough $N_{sat}N_{sat}$ pairs, this should imply less power at small scales.

The data set that probes the smallest scales is represented by Richardson et al. (2012). Here only the DI prediction with the highest normalization of the inflow shows a clear departure from small-scale data and from the IT prediction; however, the good match of the two other DI predictions should not considered as conclusive. As shown by the AGN MOF in Sect 5.1, these two models underpredict the number density of luminous AGN at every halo mass, also missing the very luminous AGN in central galaxies in $10^{12} \sim 10^{13} h^{-1} M_\odot$ dark matter halos. This gives more power to small scales, but at the same time implies that the two predictions can only account for a small fraction of the luminous AGN sample we compared with.

In the two other comparisons that partially probe the small scale regime (Krumpe et al. 2010 and Shen et al. 2013), the DI mode always shows less power at small scales with respect to the IT model, especially in the former comparison. Indeed, at low redshift the drop in the high-mass end of central active galaxies of the DI scenario becomes more relevant, since massive environments are more common, substantially affecting the small scale clustering. In the comparison with Shen et al. (2013), the cross-correlation with the galaxy sample partially mitigate the differences between the two models.

More data are needed to further test our models in reproducing small scales clustering, also at higher redshift (where DIs increase their efficiency and might reverse the trend with the IT mode). The 1-halo term can provide information on the efficiency of distinct triggering modes, since it is quite sensible to differences in the relative distribution of central and satellite AGN. However, its analysis should always be followed by the study of other complimentary observables (e.g., MOF directly measured, pairwise velocity distribution), in order to give more stringent constraints on the AGN satellite fraction and to break the degeneracies in the HOD modeling.

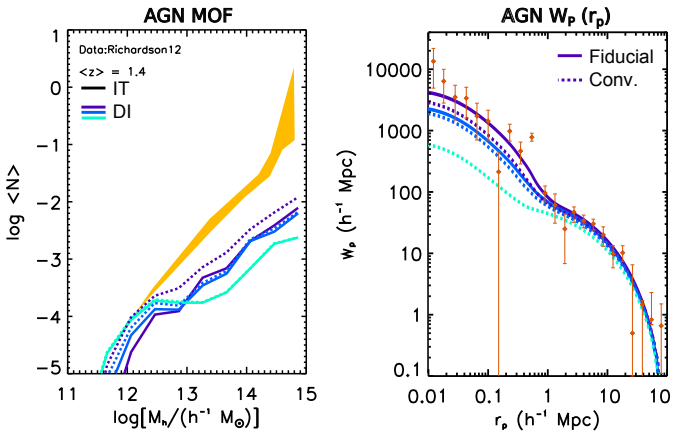

Figure 10. AGN MOF and 2PCF for the DI scenario after having matched the AGN luminosity function bright-end (dotted lines). Continuous lines represent the fiducial predictions. Data from Richardson et al. (2012)

6 DISCUSSION

6.1 DI scenario: robustness of results

One of the main prediction we obtained for the DI scenario is that DIs fall short in triggering central AGN in massive halos, with AGN in satellites not being enough to match the observational constraints. As a first test, we check whether the lack of DI AGN in massive halos might be due to observational statistical errors. The DI models have in fact the tendency to underproduce the bright end of the AGN luminosity function (Menci et al. 2014), and in turn the distribution of luminous AGN in massive halos. At least part of this shortfall in these type of models may be attributable to random errors in the observed luminosities. To check for this, we convolved our mock AGN catalogs with Gaussian errors. Being interested in the maximal effect of this procedure, we have forced the bright end of the predicted LF to match the observed one, regardless of the assumed width of the Gaussian errors. For reference purposes, we have used for the DI prediction with $\alpha = 10$ ($\alpha = 2$) a dispersion of width $\delta LogL_{1450} = 0.2$ mag ($\delta LogL_{1450} = 0.8$ mag) at $z \lesssim 1$, increasing to $\delta LogL_{1450} = 0.8$ mag ($\delta LogL_{1450} = 1.8$ mag) at $z \sim 2.5$.

Fig. 10 shows the effects of such procedure on the AGN MOF and 2PCF. The global effect of including a scatter in the AGN luminosities on the AGN MOF and on the 2PCF are minor, though not negligible, with the predicted clustering strength decreasing with increasing scatter, as expected (e.g., Haiman et al. 2001; Martini & Weinberg 2001; Shankar et al. 2010). Overall, we believe that the underproduction of the DI models in producing luminous AGN is a true physical effect, caused by the low gas and disk fractions in massive galaxies.

The lack of AGN in central galaxies residing in massive dark matter halos, as well as the high AGN satellite fraction, are caused mainly by the triggering criterion and to a less extent by the model for the mass inflow, but should be considered general features of the DI scenario regardless of its precise modeling. The key point is that central galaxies are always more massive than satellites at a fixed dark matter halo mass. Since in massive galaxies the disk and gas fractions decrease, at a fixed halo mass the ideal conditions to trigger DIs should be found in satellites rather than in centrals. This is also supported by observations. For instance Bluck et al. (2014)

find that the fraction of passive SDSS galaxies at low redshift is higher in centrals than in the satellites of the same dark matter halo.

We stress that our modeling needs a triggering criterion: the type of gas inflows taken into account here (eq. 5) are meant to arise specifically in response to large-scale strong torques on gas from non-axisymmetric perturbations to the stellar gravitational potential (Hopkins & Quataert 2011). It could be interesting to explore different modelizations of the DI scenario. For example, we could decouple the triggering on the central black hole from the large-scale disk instability by assigning gas accretion onto the black hole at a certain rate (for example given by Eq. 5) simply as long as there is enough gas mass present in the disk. In some respect, this is what envisioned in clumpy accretion models (e.g., Dekel et al. 2009; Bournaud et al. 2011). We will explore clumpy accretion in future work.

6.2 AGN MOF parametric form

The shape and the parametric form assumed by the AGN MOF is also a critical issue. In the literature the AGN mean occupation function is often described as a softened step function for the central component plus a rolling-off power law for the satellite component, even if other parametric forms have been investigated (Miyaji et al. 2011; Chatterjee et al. 2012; Richardson et al. 2012; Kayo & Oguri 2012; Shen et al. 2013).

The details of the total AGN MOF predicted by our SAM generally depends on the specific triggering mechanism and on the ranges of luminosity and redshift considered. For the MOF of central AGN, in agreement with the findings of other authors, we obtain that the 2PCF poorly constrains the AGN MOF high-mass end. A drop in the central MOF in massive environments, such as in the case of the DI scenario, little affects the AGN 2PCF, especially at high redshift.

Another important issue concerns the AGN duty cycle. In some cases, the step function of the central MOF is modeled in a way that at $M_h \sim 10^{14} - 10^{15}\mathrm{M}_\odot$ saturates to unity (e.g. Richardson et al. 2013). Here we note that this approach might be incorrect. Indeed, it would imply that every massive halo hosts an AGN in the central galaxy, regardless of the luminosity cut used for the sample. While this assumption is plausible for inactive galaxies, the parametric expression for central AGN should require a different parameterization, accounting also for a mass-dependent AGN duty cycle. In all the samples we compared with our predictions favor this latter approach, since they never saturate to unity at the high-mass end.

As for the satellite MOF, the situation is more complex. Observationally, it is mainly constrained by the small-scale clustering, which is particular difficult to probe. In previous works, it has been parameterized mainly as a rolling-off power-law, but there is no general consensus on the exact value of the exponent, which is largely uncertain. Shen et al. (2013) obtained a value for the exponent of $\alpha = 1.19^{+0.37}_{-0.33}$; Richardson et al. (2013), otherwise, obtained an higher value of $\alpha = 2.59^{+0.33}_{-1.87}$. The best fit value of Chatterjee et al. (2013) is $\alpha = 1.03 \pm 1.12$, even if their slope remains completely unconstrained. Chatterjee et al. (2012) obtained slightly lower values in the range $0.3 \sim 1.4$, while Leauthaud et al. (2015) suggested a value for the exponent close to unity. We stress again that the normalization and the precise shape of the AGN MOF depends on the particular sample we compare with. However, the general trend of our SAM seems to favor a picture where the satellite MOF is described by a power law with exponent $\alpha = 0.5 \sim 1$ (thus excluding higher values), and a cut-off towards lower dark matter halo masses, mainly dependent on the exact host galaxy stellar mass/luminosity cut.

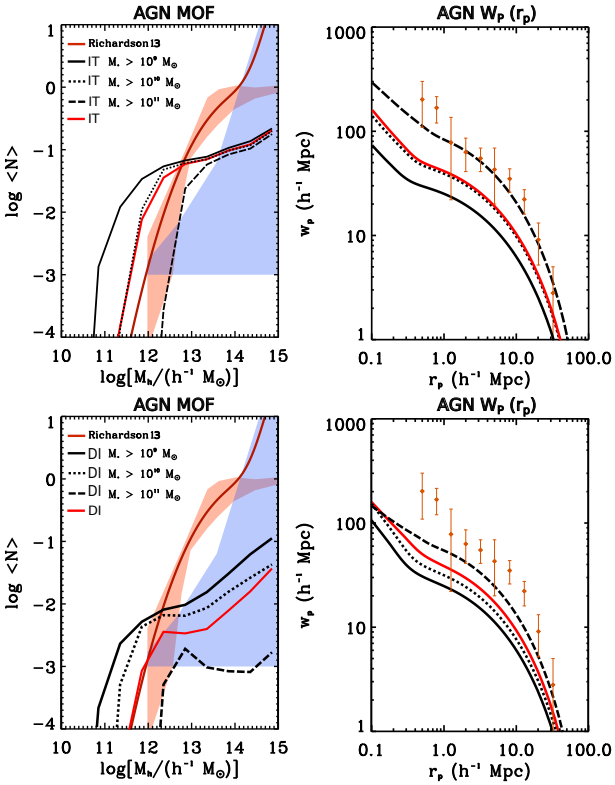

Figure 11. AGN MOF and 2PCF for the IT and DI scenarios concerning the comparison with Richardson et al. (2013) data. The continuous red lines represent the fiducial predictions for the IT and DI scenarios obtained considering the full redshift and luminosity interval of the sample, as well as the cut on the host galaxy magnitude of $I_{AB} < 23$. The continuous, dashed and dotted black lines have been obtained instead substituting the condition on the host galaxy magnitude ($I_{AB} < 23$) with a cut on the host galaxy stellar mass of $Log M_* > 9, 10, 11\mathrm{M}_\odot$.

6.3 Effects of selection cuts

We finally test the effect of using different selection cuts on the AGN MOF and 2PCF.

In order to do so, we compare our predictions with the AGN 2PCF from Richardson et al. (2013) and the associated AGN MOF obtained using the HOD modeling. The authors considered a sample of XMM-COSMOS AGN in the redshift range of $0 < z < 4 (< z >= 1.2)$, with typical luminosities in the range of $L_X \sim 41 - 45$, and with a magnitude cut for AGN host galaxies of $I_{AB} < 23$. These broad selection intervals are ideal to test the impact of diverse observational cuts on the models outputs.

At face value, the IT and DI scenario fail in reproducing both the 2PCF and the AGN MOF inferred by the authors. In particular, the average halo mass predicted by our models is in the range $Log M_h \sim 12.2 - 12.4$, at odds with the $Log M_h \sim 13$ derived by Richardson et al. (2013).

Given the large redshift and luminosity intervals spanned by their sample, the discrepancy might at least in part be induced by not properly accounting for the non-trivial selection functions inherent in the observational sample. In fig. 11 we check how the

AGN MOF and 2PCF are influenced by different selection cuts specifically in terms of host galaxy stellar mass. As displayed by fig. 11, considering only the most massive host galaxies affects the AGN MOF and 2PCF (as already highlighted in Sect 4.2), resulting into an increment of the AGN bias and a better match to the observed 2PCF. The match is improved in the IT model when selecting galaxies with stellar mass $M_* > 10^{11}\mathrm{M}_\odot$. The effect is slightly less pronounced in the DI scenario, since DIs are effective only in a limited range of host galaxy stellar masses ($LogM_* < 11.5\mathrm{M}_\odot$).

Fig. 11 clearly highlights the importance of properly taking into account selection cuts in the host galaxy population (such as stellar mass), especially when comparing results concerning AGN selected at different wavelengths. Indeed, the higher X-ray clustering signal, which has been often interpreted as an additional channel for AGN triggering, might be understood in terms of selection biases and in terms of the properties of the underlying host galaxy population.

This view is also supported by the recent paper of Mendez et al. (2015). Studying the clustering properties of X-ray, radio, and mid-IR AGN from the PRIMUS and DEEP2 redshift surveys, they found a higher clustering signal for X-ray and radio AGN with respect to mid-IR selected AGN. Nonetheless, the differences disappeared when comparing the clustering of each AGN sample with matched galaxy samples with similar properties in terms of stellar mass, star formation, redshift.

7 CONCLUSIONS

Using an advanced semi analytic model (SAM) for galaxy formation (Menci et al. 2014; Gatti et al. 2015), coupled to accurate halo occupation distribution modeling, we have investigated the imprint left by different AGN triggering mechanisms on the clustering strength of the AGN population at small and large scales. Two fueling mechanisms have been considered: a first accretion mode where AGN activity is triggered by disk instabilities (DI scenario) in isolated galaxies, and a second feeding mode where galaxy mergers and fly-by events (IT scenario) are responsible for producing a sudden destabilization of large quantities of gas, causing the mass inflow onto the central SMBH. The final goal of this paper was to highlight key features in the clustering properties of the two modes that might constitute robust probes to pin down the dominant SMBH fueling mechanism. We obtained the following results:

(i) DIs, irrespective of their exact implementation in the SAM, tend to fall short in triggering AGN activity in galaxies at the center of halos with $M_h > 10^{13.5}h^{-1}\mathrm{M}_\odot$ (at all redshifts). For centrals in less massive environments, DI are particularly effective in triggering $L \sim L_{knee}$ AGN. On the contrary, the IT scenario predicts abundance of active, central galaxies that generally agrees well with observations at every halo mass, for a wide range of AGN luminosities and redshift.

(ii) The relative number of satellites in DIs at intermediate-to-low luminosities is always significantly higher than in IT models, especially in groups and clusters, indicating a preference of DI AGN to inhabit satellite galaxies. However, the absolute abundance of satellite AGN at $z \lesssim 1$ is still underpredicted by DI models.

(iii) Similarly, the low-satellite fraction predicted for the IT scenario would suggest that different feeding modes might partially contribute to the triggering of satellite AGN in groups and clusters, at least for intermediate-to-low luminosities at $z \lesssim 1$.

(iv) Both scenarios are quite degenerate in matching large-scale clustering measurements, concerning both X-ray and optically selected AGN surveys, with different average luminosity and redshift. This seems to indicate that the sole analysis of the large scale clustering (i.e. bias factor) constitutes a poor constraint of the DI and IT modes.

(v) Selection cuts in terms of AGN luminosity, host galaxy properties, redshift interval might have a more relevant role in driving the differences often observed in the bias factor inferred from surveys carried out at different wavelengths.

(vi) Our analysis suggests the presence of both a mild luminosity and a more consistent redshift dependence of the AGN clustering: at $z \sim 0.5$ luminous AGN are hosted by halos with mass $10^{12} - 10^{13}\mathrm{M}_\odot$, while moderately luminous AGN occupy a wide range of dark matter halos of different mass. Less luminous AGN are biased towards lower dark matter halo masses. At high redshift, the average halo mass sensibly moves towards lower values.

Our analysis suggests the need of new AGN host halo mass distributions possibly directly probed via, e.g., lensing or dynamical measurements, and possibly with clearer selections on the host galaxy properties, where possible.

References

Abazajian K. N., et al., 2009, ApJS, 182, 543
Adelman-McCarthy J. K., et al., 2007, ApJS, 172, 634
Aird J., et al., 2012, ApJ, 746, 90
Allevato V., et al., 2011, ApJ, 736, 99
Allevato V., et al., 2012, ApJ, 758, 47
Allevato V., et al., 2014, ApJ, 796, 4
Angulo R. E., Lacey C. G., Baugh C. M., Frenk C. S., 2009, MNRAS, 399, 983
Arp H., 1970, AJ, 75, 1
Baugh C. M., 2006, Reports on Progress in Physics, 69, 3101
Berlind A. A., et al., 2003, ApJ, 593, 1
Bessiere P. S., Tadhunter C. N., Ramos Almeida C., Villar Martín M., 2012, MNRAS, 426, 276
Bluck A. F. L., Mendel J. T., Ellison S. L., Moreno J., Simard L., Patton D. R., Starkenburg E., 2014, MNRAS, 441, 599
Bond J. R., Cole S., Efstathiou G., Kaiser N., 1991, ApJ, 379, 440
Bongiorno A., et al., 2012, MNRAS, 427, 3103
Bonoli S., Shankar F., White S. D. M., Springel V., Wyithe J. S. B., 2010, MNRAS, 404, 399
Bournaud F., Dekel A., Teyssier R., Cacciato M., Daddi E., Juneau S., Shankar F., 2011, ApJ, 741, L33
Cappelluti N., Ajello M., Burlon D., Krumpe M., Miyaji T., Bonoli S., Greiner J., 2010, ApJ, 716, L209
Cappelluti N., Allevato V., Finoguenov A., 2012, Advances in Astronomy, 2012, 1
Chatterjee S., Degraf C., Richardson J., Zheng Z., Nagai D., Di Matteo T., 2012, MNRAS, 419, 2657
Chatterjee S., Nguyen M. L., Myers A. D., Zheng Z., 2013, ApJ, 779, 147
Civano F., et al., 2012, ApJS, 201, 30
Coil A. L., Hennawi J. F., Newman J. A., Cooper M. C., Davis M., 2007, ApJ, 654, 115
Coil A. L., et al., 2009, ApJ, 701, 1484
Combes F., et al., 2009, A&A, 503, 73
Cooray A., Sheth R., 2002, Phys. Rep., 372, 1
Cox T. J., Jonsson P., Somerville R. S., Primack J. R., Dekel A., 2008, MNRAS, 384, 386
Croom S. M., Smith R. J., Boyle B. J., Shanks T., Miller L., Outram P. J., Loaring N. S., 2004, MNRAS, 349, 1397
Davis M., Peebles P. J. E., 1983, ApJ, 267, 465
Dekel A., et al., 2009, Nature, 457, 451
Di Matteo T., Springel V., Hernquist L., 2005, Nature, 433, 604
Di Matteo T., Colberg J., Springel V., Hernquist L., Sijacki D., 2008, ApJ, 676, 33
Efstathiou G., Lake G., Negroponte J., 1982, MNRAS, 199, 1069

Elvis M., et al., 2009, ApJS, 184, 158
Fanidakis N., Baugh C. M., Benson A. J., Bower R. G., Cole S., Done C., Frenk C. S., 2011, MNRAS, 410, 53
Finoguenov A., et al., 2007, ApJS, 172, 182
Gatti M., Lamastra A., Menci N., Bongiorno A., Fiore F., 2015, A&A, 576, A32
Gehrels N., 1986, ApJ, 303, 336
George M. R., et al., 2011, ApJ, 742, 125
Gruppioni C., et al., 2015, MNRAS, 451, 3419
Haiman Z., Mohr J. J., Holder G. P., 2001, ApJ, 553, 545
Hennawi J. F., et al., 2006, AJ, 131, 1
Hickox R. C., et al., 2009, ApJ, 696, 891
Hopkins P. F., Quataert E., 2011, MNRAS, 415, 1027
Hopkins P. F., Hernquist L., Cox T. J., Kereš D., 2008, ApJS, 175, 356
Hopkins P. F., Kocevski D. D., Bundy K., 2014, MNRAS, 445, 823
Kauffmann G., Nusser A., Steinmetz M., 1997, MNRAS, 286, 795
Kayo I., Oguri M., 2012, MNRAS, 424, 1363
Koester B. P., et al., 2007, ApJ, 660, 239
Komatsu E., et al., 2009, ApJS, 180, 330
Kormendy J., Ho L. C., 2013, ARA&A, 51, 511
Koss M., Mushotzky R., Veilleux S., Winter L., 2010, ApJ, 716, L125
Koutoulidis L., Plionis M., Georgantopoulos I., Fanidakis N., 2013, MNRAS, 428, 1382
Krumpe M., Miyaji T., Coil A. L., 2010, ApJ, 713, 558
Krumpe M., Miyaji T., Coil A. L., Aceves H., 2012, ApJ, 746, 1
Lacey C., Cole S., 1993, MNRAS, 262, 627
Landy S. D., Szalay A. S., 1993, ApJ, 412, 64
Läsker R., Ferrarese L., van de Ven G., Shankar F., 2014, ApJ, 780, 70
Leauthaud A., et al., 2007, ApJS, 172, 219
Leauthaud A., et al., 2010, ApJ, 709, 97
Leauthaud A., et al., 2015, MNRAS, 446, 1874
Lidz A., Hopkins P. F., Cox T. J., Hernquist L., Robertson B., 2006, ApJ, 641, 41
Lutz D., et al., 2010, ApJ, 712, 1287
Magorrian J., et al., 1998, AJ, 115, 2285
Marconi A., Hunt L. K., 2003, ApJ, 589, L21
Marconi A., Risaliti G., Gilli R., Hunt L. K., Maiolino R., Salvati M., 2004, MNRAS, 351, 169
Martini P., Weinberg D. H., 2001, ApJ, 547, 12
Martini P., Sivakoff G. R., Mulchaey J. S., 2009, ApJ, 701, 66
McConnell N. J., Ma C.-P., 2013, ApJ, 764, 184
McIntosh D. H., Guo Y., Mo H. J., van den Bosch F., Yang X., 2009, in American Astronomical Society Meeting Abstracts #213. p. 423.09
Menci N., Cavaliere A., Fontana A., Giallongo E., Poli F., Vittorini V., 2004, ApJ, 604, 12
Menci N., Fontana A., Giallongo E., Grazian A., Salimbeni S., 2006, ApJ, 647, 753
Menci N., Fiore F., Puccetti S., Cavaliere A., 2008, ApJ, 686, 219
Menci N., Gatti M., Fiore F., Lamastra A., 2014, A&A, 569, A37
Miyaji T., Krumpe M., Coil A. L., Aceves H., 2011, ApJ, 726, 83
Mo H. J., Mao S., White S. D. M., 1998, MNRAS, 295, 319
Moster B. P., Naab T., White S. D. M., 2013, MNRAS, 428, 3121
Mullaney J. R., et al., 2012, MNRAS, 419, 95
Myers A. D., et al., 2006, ApJ, 638, 622
Padmanabhan N., White M., Norberg P., Porciani C., 2009, MNRAS, 397, 1862
Pentericci L., et al., 2013, A&A, 552, A111
Porciani C., Magliocchetti M., Norberg P., 2004, MNRAS, 355, 1010
Press W. H., Schechter P., 1974, ApJ, 187, 425
Richards G. T., et al., 2006, AJ, 131, 2766
Richardson J., Zheng Z., Chatterjee S., Nagai D., Shen Y., 2012, ApJ, 755, 30
Richardson J., Chatterjee S., Zheng Z., Myers A. D., Hickox R., 2013, ApJ, 774, 143
Richstone D., et al., 1998, Nature, 395, A14
Rosario D. J., et al., 2012, A&A, 545, A45
Rosario D. J., et al., 2013, ApJ, 763, 59
Rykoff E. S., et al., 2012, ApJ, 746, 178
Salvato M., et al., 2011, ApJ, 742, 61
Sanders D. B., Mirabel I. F., 1996, ARA&A, 34, 749
Santini P., et al., 2012, A&A, 540, A109
Saslaw W. C., 1985, Gravitational physics of stellar and galactic systems
Satyapal S., Ellison S. L., McAlpine W., Hickox R. C., Patton D. R., Mendel J. T., 2014, MNRAS, 441, 1297
Schlegel D., White M., Eisenstein D., 2009, in astro2010: The Astronomy and Astrophysics Decadal Survey. p. 314 (arXiv:0902.4680)
Schneider D. P., et al., 2010, AJ, 139, 2360
Shankar F., Salucci P., Granato G. L., De Zotti G., Danese L., 2004, MNRAS, 354, 1020
Shankar F., Lapi A., Salucci P., De Zotti G., Danese L., 2006, ApJ, 643, 14
Shankar F., Weinberg D. H., Miralda-Escudé J., 2009, ApJ, 690, 20
Shankar F., Crocce M., Miralda-Escudé J., Fosalba P., Weinberg D. H., 2010, ApJ, 718, 231
Shankar F., Weinberg D. H., Miralda-Escudé J., 2013, MNRAS, 428, 421
Shankar F., et al., 2014, ApJ, 797, L27
Shen Y., et al., 2007, AJ, 133, 2222
Shen Y., et al., 2013, ApJ, 778, 98
Sheth R. K., Tormen G., 1999, MNRAS, 308, 119
Soltan A., 1982, MNRAS, 200, 115
Starikova S., et al., 2011, ApJ, 741, 15
Tinker J. L., Weinberg D. H., Zheng Z., Zehavi I., 2005, ApJ, 631, 41
Treister E., Schawinski K., Urry C. M., Simmons B. D., 2012, ApJ, 758, L39
Ueda Y., Akiyama M., Hasinger G., Miyaji T., Watson M. G., 2014, ApJ, 786, 104
Urrutia T., Lacy M., Spoon H., Glikman E., Petric A., Schulz B., 2012, ApJ, 757, 125
Vale A., Ostriker J. P., 2004, MNRAS, 353, 189
Villforth C., et al., 2014, MNRAS, 439, 3342
Voges W., et al., 1999, A&A, 349, 389
White M., Martini P., Cohn J. D., 2008, MNRAS, 390, 1179
White M., et al., 2011, ApJ, 728, 126
White M., et al., 2012, MNRAS, 424, 933
Xia J.-Q., Negrello M., Lapi A., De Zotti G., Danese L., Viel M., 2012, MNRAS, 422, 1324
Yu Q., Tremaine S., 2002, MNRAS, 335, 965
Zheng Z., Weinberg D. H., 2007, ApJ, 659, 1

APPENDIX A: HALO MODEL

With the halo model (Kauffmann et al. 1997; Cooray & Sheth 2002; Tinker et al. 2005; Zheng & Weinberg 2007) it is possible to reformulate the pieces of information provided by clustering analysis concerning the spatial distribution of AGN into an accurate description of how AGN populate dark matter halos with different mass. The key element of the halo model is constituted by the halo occupation distribution (HOD), which is defined as the conditional probability $P(N|M_h)$ that an halo of mass M_h contains N AGN. If the AGN HOD is known, under a set of assumptions the large-scale bias factor, the average halo mass and the 2PCF relative to the AGN sample are readily computable.

Usually the AGN HOD is obtained indirectly from clustering measurements: once having assumed a parametric expression, the 2PCF is used to constrain the parameters of the HOD. The full P(N|M) could be specified by determining all its moments observationally from AGN clustering at each order; unfortunately, due to the paucity of AGN, it is not possible to accurately measure higher order statistics (such as 3PCF).

The problem is solved by using an approximate description of the halo model and considering only the two lowest-order moments, namely $\langle N(M_h)\rangle$ (also known as mean occupation function, MOF) and $\langle N(N-1)\rangle_{M_h}$. The mean occupa-

tion function, defined as $\langle N(M_h)\rangle = \Sigma_N NP(N|M_h)$, is usually expressed as the sum of a central and satellite components $\langle N(M_h)\rangle = \langle N(M_h)\rangle_{cen} + \langle N(M_h)\rangle_{sat}$.

We made use of the following equations to relate the AGN MOF to the AGN average bias factor and 2PCF. By assuming a halo mass function $n(M_h)$ (Press & Schechter 1974; Sheth & Tormen 1999) and a halo bias factor $b(M_h)$ one can obtain

$$n_{AGN} = \int n(M_h)\langle N(M_h)\rangle dM_h, \tag{A1}$$

$$b_{AGN} = n_{AGN}^{-1} \int n(M_h)\langle N(M_h)\rangle b(M_h) dM_h, \tag{A2}$$

$$\langle M_h\rangle = n_{AGN}^{-1} \int n(M_h)\langle N(M_h)\rangle M_h dM_h, \tag{A3}$$

which are the AGN number density, the effective bias factor and the effective halo mass for the AGN sample considered.

As for the AGN 2PCF, according to the halo model it can be thought as the sum of two contributions: the 1-halo term $\xi_{1-h}(r)$, exclusively due to the contribution of AGN residing in the same halo, and the 2-halo term $\xi_{2-h}(r)$, due to the correlation of objects residing in different halos. The 1-halo term can be computed as follows (Berlind et al. 2003):

$$\xi_{1-h}(r) = \frac{1}{4\pi r^2 n_{AGN}} \int n(M_h) \frac{\langle N(N-1)\rangle}{2R_{vir}} F'\left(\frac{r}{2R_{vir}}\right) dM_h, \tag{A4}$$

with R_{vir} being the virial radius of a halo of mass M_h and F' the radial derivative of the NFW profile of the dark matter halo. The terms $\langle N(N-1)\rangle$ and F' have been computed following Zheng & Weinberg (2007). The 2-halo term is instead computed using

$$\xi_{2.h}(r) = \frac{1}{2\pi^2} \int P_{2-h}(k,r) k^2 \frac{sin(kr)}{kr} dk, \tag{A5}$$

with

$$P_{2-h}(k,r) = \frac{P_m(k)}{n_{AGN}^2} \left[\int n(M_h) b(M_h) y(k,M_h) dM_h\right]^2, \tag{A6}$$

where $y(k,M_h)$ represents the Fourier transform of the NFW profile, computed following Xia et al. (2012), and $P_m(k)$ the matter power spectrum. It is worth noting that since at large scales $y \to 1$, $P_{2-h}(k,r) \approx b_{AGN}^2 P_m(k)$ (Cappelluti et al. 2012). Ultimately, we note that to compare with observations the 2PCF $\xi(r)$ can be converted into the projected 2PCF $w_p(r_p)$ using the Abel transform (Davis & Peebles 1983):

$$w_p(r_p) = 2 \int_0^\infty \xi\left(\sqrt{r_p^2 + y^2}\right) dy \tag{A7}$$

APPENDIX B: REDSHIFT AND LUMINOSITY DEPENDENCE OF AGN CLUSTERING: PREVIOUS OBSERVATIONAL RESULTS

Several authors have investigated the luminosity and redshift evolution of AGN clustering measurements. Shen et al. (2013), dividing their $< z >= 0.5$ sample in different luminosity bins in the range $-23.5 < m_i < -25.5$, found weak/no sign of luminosity evolution in their clustering measurements, even if they cannot completely rule out stronger evolution, given their uncertainties. Similar results have been found by Chatterjee et al. (2013), at a slightly lower redshift. Richardson et al. (2012) have shown that dividing their $< z >= 1.4$ sample of luminous AGN in two sub-samples above and below the median redshift little affects the AGN 2PCF, hence suggesting no strong redshift evolution. No redshift evolution has been also found by Allevato et al. (2011), who showed that moderately luminous XMM COSMOS AGN reside in dark matter halos with constant mass up to $z \sim 2$. On the contrary, Chatterjee et al. (2012), with their cosmological hydrodynamic simulation, suggested a strong redshift and luminosity evolution of the AGN HOD in the redshift interval $z \sim 1-3$, but they focused on lower bolometric luminosities in the range $10^{38} - 10^{42}$ ergs^{-1}. Allevato et al. (2014) found that COSMOS AGN at $z \sim 3$ inhabit less massive dark matter halos with respect to their low redshift counterparts, suggesting a redshift evolution for $z > 2$. Ultimately, Koutoulidis et al. (2013), focusing on moderately luminous X-ray AGN in the redshift range $0 < z < 3$, noticed no strong redshift evolution up to $z \sim 1.5$, but they found a positive dependence of the bias factor on AGN X-ray luminosity. Particularly, in their picture at redshift $z \sim 1$ moderately luminous AGN with L_X up to 10^{44} ergs^{-1} inhabit more massive halos ($M_h \sim 10^{13}$M$_\odot$) with respect to less luminous AGN; the authors furthermore suggest that high luminosity AGN ($L_X > 10^{44}$ ergs^{-1}) might also occupy less massive halos with $M_h \sim 10^{12}$M$_\odot$, in agreement with clustering measurements of luminous QSOs.

APPENDIX C: DATA DESCRIPTION AND SELECTION CUTS USED IN SECT. 5

C1 AGN MOF from 2PCF measurements

The left three panels of fig. 7 represents the comparison with data from Shen et al. (2013), who obtained the AGN MOF from a 2-point AGN-galaxy cross correlation function (CCF) measurement. They considered a subset of optically-selected quasars in the SDSS DR7 quasar catalog (Abazajian et al. 2009; Schneider et al. 2010), in the redshift range $0.3 < z < 0.9$ with median redshift $< z >= 0.53$. The quasar sample is flux limited to $i < 19.1$, with a median luminosity of $LogL_{bol} \approx 45.5$ erg s^{-1} (roughly corresponding to $\approx L_{knee}$). As for the galaxy sample, they considered the DR10 CMASS galaxy sample (White et al. 2011) from the Baryonic Oscillation Spectroscopic Survey (Schlegel et al. 2009).

The right panel represents the comparison with data taken from Richardson et al. (2012). The authors firstly obtain the AGN 2PCF by combining an AGN sample from SDSS DR7 on large scale and a binary quasar sample take from Hennawi et al. (2006) relative to small scales; then, by applying the halo model formalism, the AGN MOF showed in fig 7 is obtained. The AGN large-scale sample span a redshift range $0.4 < z < 2.5$, with a median redshift of $< 1.4 >$, and is flux limited to $i < 19.1$. The binary quasar sample, relative to scales $r_p < 20$ h^{-1}kpc, has been obtained by detecting faint companions (flux limited to $i < 21.0$) around a parent sample of SDSS DR3 and 2QZ (Croom et al. 2004) quasars, and is characterized by a slightly higher median redshift ($< z >= 1.6$). The average luminosity of the sample is very high, approximately $logL_{bol} \approx 46.4$.

To compare with the AGN sample from Richardson et al. (2012), we have chosen to use the redshift and luminosity cut associated with the large-scale sample ($0 < z < 2.5$ and $i < 19.1$) for AGN in central galaxies, while AGN in satellites have been selected

in the same redshift range but with a lower luminosity threshold ($i < 21$), so as to mimic the selection cut of the small-scale sample.

C2 AGN MOF from direct measurements and SHMR-based approach

The upper left panels of fig. 8 show data from Allevato et al. (2012), who considered 41 XMM-COSMOS (Salvato et al. 2011) and 17 C-COSMOS (Elvis et al. 2009) AGN with photometric and spectroscopic redshift at $z \leq 1$, and associated them with member galaxies of X-ray detected galaxy groups in the COSMOS field (Finoguenov et al. 2007) to obtain the AGN HOD. Group masses have been assigned from an empirical mass-luminosity relation (Leauthaud et al. 2010), and are in the range $LogM_h \sim 10^{13} - 10^{14.2} M_\odot$. AGN have been assigned to central and satellite galaxies by cross-matching the AGN sample with galaxy membership catalogs (Leauthaud et al. 2007; George et al. 2011). The authors also tried to take into account the luminosity and redshift dependence of their sample, by properly correcting the AGN HOD with a weight factor. Particularly, their weight factor considered both the fact that they were including AGN with luminosity lower than $L_{X(0.1-2.4KeV)} < 10^{42.2}$ ergs^{-1} (which is the luminosity threshold at the highest redshift probed by their sample) and the redshift evolution of the AGN number density. To compare with their data, we selected AGN in the redshift range $0 < z < 1$ with $L_{X(0.1-2.4KeV)} > 10^{42.2}$ ergs^{-1} and corrected the AGN number density at different redshifts with a weight factor accounting for the redshift evolution similar to the one adopted by Allevato et al. (2012). Given the low redshift range and the high dark matter halo mass probed here, no additional cut on the host galaxy stellar mass have been applied, since it would not affect the AGN MOF.

Chatterjee et al. (2013) (upper right panel) used SDSS DR7 quasars and galaxy group catalogs from MaxBCG sample (Koester et al. 2007) to empirically measure the HOD of quasars at low redshift. They used a subsample of SDSS quasars in the redshift range $0.1 < z < 0.3$ and absolute magnitude $M_i < -22$ ($LogL_{bol} \gtrsim 44.7$). The MaxBGC sample contains galaxy groups and clusters with velocity dispersion greater than ~ 400 km/s, in the redshift range $0.1 < z < 0.3$. Groups and clusters are obtained by identifying first the brightest cluster galaxies (BCGs), and then by assigning group members by selecting those galaxies that lie within R_{gal200} (defined as the radius within which the galaxy density is 200 times higher than background) of a BCG. The group/cluster mass is then computed using the modified optical richness method of Rykoff et al. (2012), with a mass error equal to 33%. Quasars are then associated with groups and clusters depending on their positions.

Ultimately, in the lower panels we show the comparison with Leauthaud et al. (2015), who used a novel approach to obtain the AGN HOD, based on the stellar-to-halo mass relation (SHMR). The authors focused on a sample of moderately luminous AGN from the XMM-COSMOS and C-COSMOS X-ray catalogs. The sample span the redshift interval $0.2 < z < 1$, with a median redshift of $< z >= 0.7$. Besides the luminosity cut due to the limiting flux of XMM-COSMOS and C-COSMOS surveys, the sample has been further constrained in luminosity to $10^{41.5}$ erg s^{-1} $< L_{X,0.5-10keV} < 10^{43.5}$ erg s^{-1} and has a median luminosity of $< L_X >= 10^{42.7}$ erg s^{-1} (corresponding roughly to $< L_{bol} >\sim 43.6$). The authors also imposed a lower host galaxy stellar mass limit of $LogM_* > 10.5$ (with host stellar masses being obtained from a SED-fitting procedure), resulting in a median stellar host mass of $< M_* >= 1.310^{11} M_\odot$. The authors firstly showed the similarity in the host halo occupation of active and inactive galaxies of a given stellar mass, by using galaxy-galaxy lensing measurements; then, through the use of the SHMR and knowing the stellar mass of AGN host galaxy, accurate predictions of the AGN HOD have been made.

C3 AGN 2PCF measurements

The comparisons displayed in fig. 9 concern 4 AGN auto-correlation functions and one AGN-galaxy cross-correlation function. The AGN-galaxy cross-correlation function (Shen et al. 2013) and one AGN auto-correlation function (Richardson et al. 2012) concern the same data sets relative to the AGN MOFs discussed in Sect. 5.1. and Appendix C1. To these we added the comparisons with three AGN auto-correlation function from Krumpe et al. (2010), Allevato et al. (2014), and Shen et al. (2007).

The sample from Krumpe et al. (2010) concerns a low redshift ($0.16 < z < 0.36$) sample of X-ray selected broad line AGN from the ROSAT All-Sky Survey (RASS, Voges et al. 1999) with SDSS optical counterparts. The survey presents a typical flux limit of $\sim 10^{13}$ erg cm^{-2} s^{-1} (0.1-2.4 keV), with a median luminosity of the sample is $< L_{X(0.1-2.4KeV)} >= 1.510^{44}$ erg s^{-1} ($< LogL_{bol} >\approx$ 45.8). The RASS/SDSS AGN sample is reasonably complete for magnitude 15 < i < 19. The AGN 2PCF shown in fig. 8 has been extrapolated by the authors from the measured cross-correlation function with a sample of Luminous Red Galaxies (LRGs) from the SDSS DR7. In this comparison, we have selected only AGN with $n_H < 10^{22} cm^{-2}$.

The other two comparisons concern two high redshift clustering measurements, from Allevato et al. (2014) and Shen et al. (2007). Allevato et al. (2014) studied the clustering properties of a sample of 252 C-COSMOS AGN and 94 XMM-Newton AGN detected in the soft band with spectroscopic or photometric redshift. The redshift interval considered here is $2.2 < z < 6.8$, with median redshift $< z >= 2.8$; the median luminosity is equal to $< L_{bol} >\approx 10^{45.3}$ ergs^{-1} , hence corresponding to the intermediate-luminosity regime. To compare with this data set, we have selected AGN according to the Chandra soft band flux limit. Since the C-COSMOS sample is 83% spectroscopically complete at $I_{AB} < 22.5$ (Civano et al. 2012), we have applied this other cut to the magnitude of our AGN host galaxies. Shen et al. (2007) considered instead an optically-selected high redshift sample of luminous AGN from SDSS DR5 (Adelman-McCarthy et al. 2007), in the redshift interval $2.9 < z < 5.4$ (median redshift $< z >= 3.2$). The whole AGN sample is flux limited to $i < 20.2$ (which corresponds to $LogL_{bol} > 46.5$ at $z \approx 2.9$).

APPENDIX D: COMPARISON WITH DEUSS

In the following we used the Dark Energy Universe Simulation Series (DEUSS), a large ensemble of high performance cosmological Dark Matter (DM) simulations of realistic Dark Energy models that follows the gravitational evolution of billions of DM particles on volumes varying from inner halo scales to the size of the observable Universe[1]. DM halos are being detected using a Friends-of-Friends (FoF) algorithm, with a percolation factor $b = 0.2$ widely used in the literature. In the specific, we make use of two simulations with different mass resolutions developed in the concordance ΛCDM model, with cosmological parameters obtained from WMAP-5 year

[1] http://www.deus-consortium.org/

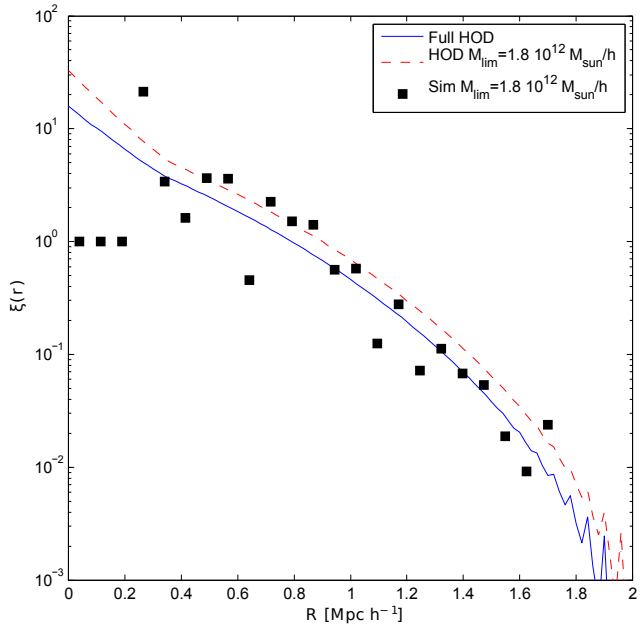

Figure D1. Comparison between the 2PCF obtained from our HOD modelling (blue and red lines) and with the one obtained using DEUSS (black dots). Both 2PCF have been obtained starting from the same AGN MOF.

data (Komatsu et al. 2009) $\Omega_\Lambda = 0.74$, $\Omega_m = 0.26$, $h = 0.72$, $n = 0.96$, $\Omega_b = 0.04$, and $\sigma_8 = 0.79$.

The numerical procedure to introduce luminous objects in a pure DM simulation is as follows. A central (resp. satellite) AGN is randomly assigned to each dark matter halo following the number density given by the AGN HOD. In order to beat the bridging effect inherent to FoF halos, the central AGN is placed at the minimum of the gravitational potential, the latter being computed from the particles detected with $b = 0.3$ FoF. We found this positioning to be equivalent to using the center of mass in 95% of DM halos. The satellites are positioned by picking randomly a DM particle belonging to the DM halo, thus ensuring we are following the right DM profile.

From this distribution, the 2PCF is estimated using the Landy & Szalay (1993) estimator. The statistical errors on the 2PCF are computed using a resampling technique based on 225 resamplings and the statistical errors drawn from a specific HOD distribution are computed through the average over 25 random HOD distributions.

Regarding the numerous systematics associated with the mass resolution and the limited volume of a simulation, we choose to use a simulation of 648 Mpc/h box length and 2048^3 particles. This simulation ensure a volume large enough to have a sufficient enough density of AGN (i.e. the n,good normalization of the 2-halo term) while maximizing the mass resolution (i.e. the accuracy on the 1-one term). The choice on the mass resolution has been made by testing our results against a 648 Mpc/h box length and 1024^3 particles simulation, which exhibits a poor resolution at small scale. The choice on the volume is obtained comparing a 2592 Mpc/h box length 2048^3 particles simulation with a smaller 648 box length and 512^3 particles simulation, at constant mass resolution. In the latter, the massive increase in volume is not changing significantly (more than a few percents) the results on the 2PCF.

This paper has been typeset from a TEX/LATEX file prepared by the author.